# Waste Form Characteristics Report

## Editors:

Ray B. Stout
Herman R. Leider

University of California
Lawrence Livermore National Laboratory
Livermore, CA 94551

Written: December 20, 1996
Issued: April 4, 1997



- Part 1

**Preface (Version 1.2)**

This version incorporates changes to several sections of the Waste Form Characteristics Report. Those sections changed are: 2.1.3.5 Dissolution Release from $UO_2$; 3.2.2 Spent Fuel Oxidation Models; 3.4.2 Spent Fuel Dissolution Models; 3.5.1 Glass Dissolution Experimental Parameters; and 3.5.2 Glass Dissolution Models. These sections were also updated in version 1.1 (August 1996). William Bourcier was responsible for updating the glass dissolution sections 3.5.1 and 3.5.2. Edward J. Kansa updated section 3.2.2 covering spent fuel oxidation models. Steven A. Steward had the responsibility for the spent fuel dissolution sections on data (2.1.3.5) and modeling (3.4.2).

The evaluation of parameters for the models is based on test data obtained by previous and ongoing testing activities at Argonne National Laboratory, Chicago, Il, Lawrence Livermore National Laboratory, Livermore, CA, and Pacific Northwest National Laboratories, Richland, WA.

Ray B. Stout

April 1997

**Preface (Version 1.0)**

Over the past several decades, sophisticated techniques have been developed to characterize the physical, thermal, chemical, mechanical, and radiological properties of nuclear radioactive waste form(s). (Here, "waste form" means the radioactive waste materials and any encapsulating or stabilizing matrix and is the definition provided by United States Nuclear Regulatory Commission in their regulation of Title 10 CFR 60.) Much of the early characterization was for design, operational efficiency, and safety of nuclear power plants. More recently, characterization activities have been directed at the design problem of safely emplacing radioactive waste form(s) in a suitable geological repository. The emplacement problem entails the team work of people from different technical disciplines; and the data exchange interface between the different technical personnel is of the utmost importance for an effective, efficient, and safe repository design. With this need in mind, we have assembled a preliminary data source of waste form characteristics. Most of the data was taken from- the open literature. The remaining data were summarized, in a preliminary form, from early results of on-going waste form testing and model development activities. In assembling the data, we hoped to address waste form related informational needs for the wide variety of technical specialists that are part of a repository design team. We have been careful not to impose any limits or restrictions on waste form response before the repository design process because only an overall design analysis or performance assessment of the waste repository system can optimize the potential design trade-off options that satisfy requirements of a geological repository containing radioactive waste form(s).

Because this is the first version of our waste form characteristics report, we expect and will welcome comments and requests for other input from users, potential users, and others who are interested in waste form information. In this way, we hope to provide and satisfy the waste form informational needs of the different technical specialists performing the design tasks for a repository. We anticipate updating this report annually with new results from our testing and model development activities as well as responding to the additional informational needs requested by users. Some deficiencies in data form and data needs have been identified and will be addressed in future revisions.

The accumulation of data was greatly facilitated because of the cooperation, interest, and esprit de corps of the following individuals, all of which we graciously acknowledge and thank: Karl Notz, Robert Einziger, Charles Wilson, Walter Gray, Harry Smith, Steve Marschman, Andrew Luksic, George Mellinger, John Bates, Les Jardine, Son Nguyen, Homer Weed, Knud Pedersen, Gregory Gdowski, Richard Van Konynenburg, William Bourcier, Carol Bruton, Stan Prussin, Andrew Zolnay, David Stahl, Richard Morissette, and Diane Harrison-Giesler. In addition, we extend a special thanks to William O'Connell for his helpful and meaningful review; Robert Day for his relentless pursuance of numerous corrections and resolution of review comments; and finally, to Sue Garber, for the fantastic job, performed with a smile, of putting the pieces together (again and again).

Ray B. Stout
Herman R. Leider

October 1991

This work performed under the auspices of the U.S. Department of Energy, Office of Civilian Radioactive Waste Management, Yucca Mountain Project, by the Lawrence Livermore National Laboratory under contract number W-7405-ENG-48.

YUCCA MOUNTAIN PROJECT

WASTE FORM CHARACTERIZATION REPORT
**VERSION 1.2**

## Section 2.1.3.5: Dissolution Radionuclide Release from $UO_2$ Fuel

**Version 1.2**
**April 4, 1997**

### 2.1.3.5.1 INTRODUCTION

The long term effects of the interactions between spent fuel, as a radioactive waste form, and groundwaters must be anticipated to safely dispose of spent fuel in an underground repository. Spent fuel dissolution and subsequent transport processes in groundwater are generally considered to be the main routes by which radionuclides could be released from a geological repository. Laboratory testing of the behavior of spent fuel under the conditions expected in a repository provides the information necessary to determine the magnitude of the potential radionuclide source term at the boundary of the fuel's cladding. Dissolution (leach) and solubility tests of spent fuel and uranium dioxide ($UO_2$) are the most important data-collection activities in spent fuel waste form testing. All work in these activities is done within the controls of an approved Quality Assurance Program. The testing is done under conditions identified by modeling Activity D-20-50 as most important in calculating release rates. Any scenarios to be used as the basis for long-term modeling are being tested to the extent possible on a laboratory scale. Spent fuel with characteristics spanning the ranges identified in Activity D-20-50 will be tested. In addition, oxidized fuel produced under Activity D-20-45 will be tested. The three dissolution activities have been separated based on the different technical techniques involved in conducting saturated (semi-static), flow-through, and unsaturated (drip) tests. The solubility tests with actinide isotopes will provide concentration limits, speciation, and potential colloidal formation for a range of ground water chemistries at temperatures which may contact the waste forms. The key outputs from these activities are the dissolution rate of irradiated fuel, the release rates of radionuclides from spent fuel, and the solution chemistry of water in contact with spent fuel.

Because $UO_2$ is the primary constituent of spent nuclear fuel, the dissolution of the $UO_2$ spent fuel matrix is regarded as a necessary first step for release of about 98% of the radioactive fission products contained within the $UO_2$ matrix. The intrinsic $UO_2$ dissolution rate sets an upper bound on the aqueous radionuclide release rate, even if the fuel is substantially degraded by other processes such as oxidation. If the fuel is substantially degraded to other oxidation states, then their dissolution responses also must be provided. The release rate is reduced for the solubility-limited actinides (U, Np, Pu and Am), which account for most of the long-lived radioactivity in spent fuel, when colloids are not present. In scenarios for the potential Yucca Mountain repository, it is assumed that the cladding has failed and water as vapor or liquid contacts the fuel. Drip tests that simulate the unsaturated

and oxidizing conditions expected at Yucca Mountain are in progress to evaluate the long-term behavior of spent nuclear fuel.

There have been many investigations of the dissolution of $UO_2$, spent fuel and uraninite (a naturally occurring $UO_2$ mineral) in aqueous solutions, under both reducing and oxidizing conditions, and as a function of various other environmental variables. Several reviews have been written, most recently by Grambow (1989). Important variables considered in the investigations included pH, temperature, oxygen fugacity, carbonate/bicarbonate concentrations, and fuel attributes. The data vary due to the differences in experimental purpose and methods, the diverse history of the fuel samples, the formation of secondary phases during the tests, the complexity of the solution and the surface chemistry of $UO_2$, and the surface area measurements of the test specimens. The results of such diverse studies are difficult to compare and interpret.

The following material summarizes the available YMP spent fuel and unirradiated uranium oxide dissolution data.

## 2.1.3.5.2 STATIC DISSOLUTION TESTS

The Series 1 tests described (Wilson 1984) were the first of several tests planned at Pacific Northwest National Laboratory (PNNL) to characterize potential radionuclide release from and behavior of spent fuel stored under YMP-proposed conditions. In the Series 1 tests, specimens prepared from Turkey Point Reactor Unit 3 fuel were tested in deionized distilled water in unsealed fused silica vessels under ambient hot cell air and temperature[1] conditions. Four specimen configurations were tested: 1) undefected fuel rod segments with water-tight end fittings, 2) fuel rod segments containing small (~200 μm diameter) laser-drilled holes through the cladding and with water-tight end fittings, 3) fuel rod segments with a machined slit through the cladding and water-tight end fittings, and 4) bare fuel particles removed from the cladding plus the cladding hulls. A "semi-static" test procedure was developed in which periodic solution samples were taken with the sample volume replenished with fresh deionized distilled water. Cycle 1 of the Series 1 tests was started during July 1983 and was 240 days in duration. At the end of the first cycle the tests were sampled, the vessels stripped in 8 M $HNO_3$, and the specimens restarted in fresh deionized distilled water for a second cycle. Cycle 2 of the Series 1 tests was terminated at 128 days in July 1984.

The Series 2 tests (Wilson 1990b) were similar to the Series 1 tests except that: 1) the Series 2 tests were run in YMP (NNWSI) reference J-13 well water, 2) each of the

[1] Hot cell temperature range is about 21°C to 28°C depending on time of year and time of day. An average value of 25°C was assumed for these ambient temperature tests.

four specimen configurations was duplicated using both the Turkey Point Reactor and H. B. Robinson Reactor PWR spent fuels, and 3) a vessel and specimen rinse procedure was added to the cycle termination procedures. Filtration of the collected rinse solution provided solids residues that were later examined for secondary-phase formation. Cycle 1 of the Series 2 tests was started in June 1984. All eight Series 2 specimens were run for a second cycle. The two bare fuel specimens were continued for Cycles 3, 4, and 5. Cycle 5 of the Series 2 bare fuel tests was terminated in June 1987 for a total five-cycle testing time of ~34 months.

The Series 3 tests (Wilson 1990a) were run for three cycles during the same approximate time period as Cycles 3, 4, and 5 of the Series 2 tests. The Series 3 tests were run in sealed stainless steel vessels and used the same four-specimen configurations used in Series 1 and Series 2 Cycles 1 and 2. Five specimens (one each of the four configurations using H. B. Robinson fuel plus an additional bare fuel specimen using Turkey Point fuel) were tested at 85°C, and a sixth specimen (H. B. Robinson bare fuel) was run at 25°C. Two additional scoping tests using preoxidized bare fuel specimens in Series-2-type silica vessels were started in August 1986. Selected results from Cycle 1 and from initial Cycle 2 samples from the oxidized fuel scoping tests were reported in Reference 4. The Series 1 and 2 tests were originally entitled "Cladding Containment Credit Tests." All of the test series were later referred to as "Spent Fuel Dissolution Tests."

Series 1 Summary

Measured releases were compared to the 10 CFR 60 inventory maximum annual release rate requirement of $10^{-5}$/year of 1000-year . Total measured release and total measured release as a fraction of inventory times $10^5$ are summarized in Table 1. The principal observations and conclusions from these spent fuel leaching tests are summarized below:

1. Within the probable accuracy of total release measurements and specimen inventory calculations, the actinides U, Pu, Am, and Cm appear to have been released congruently.

2. Limited data suggest that $^{237}Np$ may have been preferentially released rather than being congruently released with other actinides as expected. However, these data are too limited to be conclusive. Inaccuracies in ORIGEN-2 calculated $^{237}Np$ inventory and radiochemical analysis could also account for those results.

**Table 2.1.3.5-1**

**Total Measured Release as a Fraction of Inventory [ x $10^5$] [(a)] For Series 1**

| Component | Bare Fuel | Slit Defect | Holes Defect | Undefected |
|---|---|---|---|---|
| Uranium (μg) | 28.0 | 0.078 | <0.041 | <0.018 |
| | (9510) | (28) | (<14) | (<6.6) |
| $^{239+240}$Pu (nCi) | 28.0 | 0.341 | 0.069 | 0.027 |
| | (7940) | (104) | (20) | (8) |
| $^{241}$Am (nCi) | 21.7 | 0.208 | <0.030 | <0.011 |
| | (12,604) | (130) | (<18.6) | (<6.4) |
| $^{244}$Cm (nCi) | 30.0 | 0.76 | 0.039 | 0.008 |
| | (13,300) | (362) | (18.1) | (<3.9 |
| $^{237}$Np[(b)] (nCi) | 54 | 2.2 | -- | -- |
| | (4.73) | (0.2) | -- | -- |
| $^{137}$Cs (nCi) | 300[(c)] | 142.1 | 85.6 | 0.041 |
| | ($1.94x10^6$) | ($3.94x10^6$) | ($2.33x10^6$) | ($1.1x10^3$) |
| $^{99}$Tc[(d)] (nCi) | 230 | 12.1 | <6.7 | -- |
| | (900) | (51) | (<28) | -- |

(a) Total measured release given in parentheses.
(b) $^{237}$Np includes only vessel strip from initial and second runs and final solution from second run.
(c) Estimate based on maximum $^{137}$Cs activities measured in solution.
(d) $^{99}$Tc includes only final solution in a vessel strip from initial and second runs.

3. A rapid fractional release of cesium on the order of the fractional fission gas release was observed for the bare fuel, slit defect, and holes defect tests. Additional preferential cesium release, possibly from grain boundary inventory, was also noted in the second run on these specimens.

4. Observed fractional $^{99}$Tc release ranged from one order of magnitude greater relative to the actinides in the bare fuel test to almost three orders of magnitude greater fractional release relative to the actinides in the holes defect test.

5. For the actinides U, Pu, Am, and Cm, approximately two orders of magnitude less total fractional release was measured in the slit defect test relative to the bare fuel test. An additional approximate one order of magnitude reduction in actinide release was observed in the holes defect test relative to the slit defect test.

6. Apparent uranium saturation occurred at ~1 ppb in all tests. Uranium in excess of a few ppb was removed by 18 Å filtration. Most of the U, Am, and Cm in solution samples from the bare fuel test was removed by filtration.

7. Grain boundary dissolution appeared to be a major source of release. Preferential release of $^{99}Tc$ is likely a result of its segregation to the grain boundaries. Grain boundaries in the spent fuel are relatively wide and easily resolved by SEM. Grain boundaries in unirradiated $UO_2$ are tight and not resolvable on a fracture surface by SEM.

8. Spent fuel leaching behavior, as well as other chemical and mechanical behavior, is influenced by microstructural phenomena, such as localized segregation of some elements to the grain boundaries. The extent of localized radionuclide segregation is influenced by irradiation temperature and may be correlated to fission gas release. Additional segregation of radionuclides into more easily leached phases could possibly occur if the fuel structure is degraded by oxidation during long-term repository storage.

Series 2 Summary

Radionuclide releases were measured from PWR spent fuel specimens tested in YMP (NNWSI) J-13 well water in unsealed fused silica vessels under ambient hot cell air conditions (25°C). Two bare fuel specimens were tested, one prepared from a rod irradiated in the H. B. Robinson (HBR) Unit 2 reactor and the other from a rod irradiated in the Turkey Point (TP) Unit 3 reactor. Both fuels were low-gas release and moderate burnup. The specimen particle size range (2 to 3 mm) was that which occurs in the fuel as a result of thermal cracking. A semi-static test method was used in which the specimens were tested for multiple cycles starting in fresh J-13 water. Periodic water samples were taken during each cycle with the sample volume (~10% of test solution) being replenished with fresh J-13 water. The specimens were tested for five cycles for a total time of 34 months.

**Table 2.1.3.5-2. J-13 Well Water Analysis**

| Component | Concentration (μg/ml) | Concentration Component | (μg/ml) |
|---|---|---|---|
| Li | 0.042 | Si | 27.0 |
| Na | 43.9 | F | 2.2 |
| K | 5.11 | Cl | 6.9 |
| Ca | 12.5 | $NO_3$ | 9.6 |
| Mg | 1.92 | $SO_4$ | 18.7 |
| Sr | 0.035 | $HCO_3$ | 125.3 |
| Al | 0.012 | | |
| Fe | 0.006 | pH | 7.6 |

1. Series 2 actinide concentrations appeared to rapidly reach steady-state levels during each test cycle. Concentrations of Pu, Am, and Cm were dependent on filtration, with Am and Cm concentrations being affected the most by filtration, suggesting that these elements may have formed colloids. Approximate steady-state concentrations of actinide elements indicated in 0.4-μm filtered solution samples are given below.

   U -- $4 \times 10^{-6}$ to $8 \times 10^{-6}$ M (1 to 2 ppm)

   Pu -- $8.8 \times 10^{-10}$ to $4.4 \times 10^{-9}$ M (20 to 100 pCi/mL $^{239+240}$Pu)

   Am---~$1.5 \times 10^{-10}$ M (~100 pCi/mL $^{241}$Am)

   Cm -- ~$2.6 \times 10^{-12}$ M (~50 pCi/mL $^{244}$Cm)

   Np -- $2.4 \times 10^{-9}$ M (0.4 pCi/mL $^{237}$Np).

2. Actinide releases as a result of water transport should be several orders of magnitude lower than the NRC 10 CFR 60.113 release limits ($10^{-5}$ of 1000-yr inventory per year) if actinide concentrations (true solution plus colloids) in the repository do not greatly exceed the steady-state concentrations measured in 0.4-μm filtered samples. Assuming a water flux through the repository of 20 L per year per waste package containing 3140 kg of spent fuel saturates at the actinide elemental concentrations given above, the following annual fractional releases are calculated based on 1000-yr inventories for 33,000 MWD/MTHM burnup PWR fuel:

   U ($8 \times 10^{-6}$ M), $1.4 \times 10^{-8}$ per year

   Pu ($4 \times 10^{-9}$ M), ~$1 \times 10^{-9}$ per year

   Am, ~$8 \times 10^{-10}$ per year

   Cm, ~$1 \times 10^{-8}$ per year

   Np, ~$3 \times 10^{-9}$ per year.

3. Gap inventory $^{137}$Cs releases of about 0.7% of inventory in the HBR test and about 0.2% of inventory in the TP test were measured at the start of Cycle 1. Smaller initial Cycle 1 releases on the order of $10^{-4}$ of inventory were measured for $^{129}$I and $^{99}$Tc.

4. Fission product nuclides $^{137}Cs$, $^{90}Sr$, $^{99}Tc$, and $^{129}I$ were continuously released with time and did not reach saturation in solution. The continuous release rates of these soluble nuclides were relatively constant during Cycles 3, 4, and 5. During Cycle 5, the release rate for both $^{90}Sr$ and $^{129}I$ was about $5.5 \times 10^{-5}$ of inventory per year in both tests. Marginally higher continuous release rates on the order of $1 \times 10^{-4}$ of inventory per year were measured for $^{137}Cs$ and $^{99}Tc$.

5. The degree to which the soluble nuclides ($^{137}Cs$, $^{90}Sr$, $^{99}Tc$, and $^{129}I$) were preferentially released relative to the amount of congruent dissolution of the $UO_2$ matrix phase was not quantitatively measured. However, the near-congruent release of soluble nuclides in later test cycles, and the inventory ratios of these nuclides to that of uranium in initial solution samples from the later cycles (a ratio of about 2.5 for $^{137}Cs$), suggest that the fractional release rates for these nuclides may not have greatly exceeded the matrix dissolution rate. A matrix dissolution rate of about $4 \times 10^{-5}$ per year appears to be a reasonable estimate for the 2 to 3-mm size fuel particles tested based on these data.

6. The present data suggesting fuel matrix dissolution rates greater than $10^{-5}$ per year imply that demonstrating 10 CFR 60.113 compliance for soluble nuclides will involve considerations other than the durability of the spent fuel waste form, such as scenarios for low-probability water contact, a distribution of cladding/container failures over time, or very low migration rates. In time, fuel degradation resulting from oxidation and grain boundary dissolution (increasing surface area) may increase the matrix dissolution rate. Upper limits for degraded fuel matrix dissolution rates are yet to be determined.

7. Comparison to the Series 3 tests (sealed vessels) indicated that most of the $^{14}C$ released in the Series 2 tests was lost to the atmosphere as $CO_2$ and not measured. The $^{14}C$ was preferentially released in the Series 3 tests at about 1% of its inventory measured in HBR fuel samples. As an activation product derived partially from nitrogen impurities, evaluation of $^{14}C$ release relative to 10 CFR 60.113 is complicated because its inventory and distribution in fuel is not well characterized.

8. The quantities of precipitated secondary phase material observed in filter residues were significantly less than observed in the 85°C Series 3 tests. $UO_2$ and calcite were the only phases confirmed by XRD examination of a cycle termination rinse filter, with a tentative indication of haiweeite based on a single line in the XRD-pattern. Amorphous-appearing, silicon-containing phases were also observed by SEM on the rinse filters, and silicon-containing flocs were observed on filters used to filter solution samples. With the possible exception of haiweeite for uranium, phases controlling the solubility of actinide nuclides were not identified.

Series 3 Summary

Specimens prepared from pressurized water reactor fuel rod segments were tested in sealed stainless steel vessels in Nevada Test Site J-13 well water at 85°C and 25°C. The test matrix included three specimens of bare-fuel particles plus cladding hulls, two fuel rod segments with artificially defected cladding and watertight end fittings, and an undefected fuel rod section with watertight end fittings. Periodic solution samples were taken during test cycles with the sample volumes replenished with fresh J-13 water. Test cycles were periodically terminated and the specimens restarted in fresh J-13 water. The specimens were run for three cycles for a total test duration of 15 months.

Actinide concentrations (uranium, plutonium, americium, curium, and neptunium) peaked early in Cycle 1 of the bare-fuel tests and then declined to steady-state levels. Isotopes of plutonium and americium account for about 98% of the activity in spent fuel at 1,000 yr. Actinide concentrations rapidly reached stable steady-state values during Cycles 2 and 3. Steady-state activities on the order of 100 pCi/mL were measured for $^{239+240}Pu$, $^{241}Am$, and $^{244}Cm$ at 25°C, and much lower activities on the order of 1 pCi/mL were measured for these radionuclides at 85°C. Even using the higher 25°C values, the steady-state concentrations indicated for all of the actinide elements were at least three orders of magnitude below those required to meet the Nuclear Regulatory Commission (NRC) 10 CFR 60.113 controlled release requirements for any realistic water flow rate through the repository. Calcium-uranium-silicate phases that may have contributed to the control of uranium concentrations were identified in the 85°C tests. Secondary phases controlling neptunium, plutonium, americium, and curium concentrations were not identified.

Concentrations of the more soluble fission product and activation product radionuclides generally tended to increase continuously with time. An exception was $^{90}Sr$, which tended to reach maximum concentrations in the 85°C tests. Continuous release rates measured for $^{99}Tc$, $^{137}Cs$, and $^{129}I$ were generally in the $10^{-4}$ to $10^{-3}$ of inventory per year range, but the rate for $^{129}I$ was lower at 25°C. Preferential release of $^{14}C$ continued through all three test cycles for a total release of about 1% of the $^{14}C$ specimen inventory. Comparison of $^{14}C$ releases in tests conducted in sealed and unsealed vessels indicated that $^{14}C$ was released to the atmosphere, most likely as $CO_2$. Although soluble radionuclides were released at rates in excess of the NRC limit of $10^{-5}$ of inventory per year in the current tests, additional data are needed to predict long-term release rates. The degree to which soluble radionuclides are preferentially released in such tests, and the degree to which the fuel will be degraded in the repository by processes such as oxidation, are not presently known.

The following conclusions and observations are made based on the results of the YMP (NNWSI) Series 3 Spent Fuel Dissolution Tests:

1. Actinide concentrations (uranium, plutonium, americium, curium, and neptunium) generally appeared to reach steady-state levels in all three test cycles of the bare-fuel tests. Control of actinide concentrations at stable levels in solution was attributed to the achievement of a steady-state between fuel dissolution and secondary-phase formation or other mechanisms such as sorption.

2. Uranium-bearing secondary phases were found in significant amounts in filter residues from the 85°C bare-fuel tests. Formation of the calcium-uranium-silicate phase uranophane was confirmed, and haiweeite was tentatively identified. A possible indication of soddyite formation was also found in one of the filter residues. Secondary phases controlling plutonium, americium, curium, and neptunium concentrations were not identified.

3. Plutonium, americium, and curium activities measured in solution samples from the 85°C bare-fuel tests were from two to three orders of magnitude lower than those measured in unfiltered and 0.4 μm filtered samples from the 25°C test. Slightly lower uranium concentrations were also measured at 85°C in Cycles 2 and 3. Lower actinide concentrations at 85°C are attributed to faster kinetics for formation of solubility-limiting secondary phases at the higher 85°C temperature. Neptunium activities showed no significant dependence on temperature or filtration.

4. Plutonium, americium and curium activities measured in 18Å filtered samples from the 25°C bare fuel test were significantly less than those measured in unfiltered and 0.4-μm filtered samples suggesting that these elements were present as colloids in this test. The effects of filtration were generally greater for americium and curium than for plutonium. Notable reductions in americium and curium activities also occurred with 0.4 μm filtration in the 85°C bare fuel tests.

5. Steady-state actinide concentrations measured in 0.4-μm filtered samples from the 25°C bare-fuel test were at least three orders of magnitude below those necessary to meet the NRC 10 CFR 60.113 controlled release requirements based on reasonable assumed water flow rates through the repository. This result is of particular significance, since plutonium and americium isotopes account for ~98% of the activity in spent fuel at 1,000 yr, and eventual plutonium and americium concentrations may be lower than those measured in 0.4-μm filtered samples from the 25°C tests.

6. Measured uranium concentrations were consistent with those predicted by the EQ3/6 geochemical modeling code for precipitation of soddyite. Good agreement between measured and predicted concentration was obtained for

neptunium based on equilibration with $NpO_2$ at 25°C when the oxygen fugacity in the simulation was set at $10^{-12}$ bars. A broad range of concentrations that bracketed the measured values was predicted for plutonium depending upon the assumed oxygen fugacity and concentration-controlling phase. Measured americium concentrations were less than predicted based on data for equilibration with $Am(OH)CO_3$ or $Am(OH)_3$.

7. Actinide fractional releases from the bare-fuel tests were much greater than in the slit-defect or hole-defects tests. Actinide releases from the slit-defect test were somewhat greater than in the hole-defects test, with most of the difference accounted for in the Cycle 1 acid strip samples. Actinide releases in the hole-defects test were not significantly different from those measured in the undefected test.

8. The radionuclides $^{137}Cs$, $^{90}Sr$, $^{99}Tc$, $^{129}I$, and $^{14}C$ were continuously released in the bare-fuel tests at rates exceeding $10^{-5}$ of inventory per year. Of these radionuclides, only $^{90}Sr$ showed significant indications that its concentration was limited by solubility. Cesium-137 showed the greatest fractional release during Cycle 1, while $^{14}C$ showed the greatest fractional release during Cycles 2 and 3.

9. Iodine-129 release was much greater at 85°C than at 25°C. Comparison of the Series 3 test results to those from the Series 2 tests gave no indication that $^{129}I$ had been lost as $I_2$ from the unsealed Series 2 vessels. The $^{129}I$ release in the slit-defect test was equivalent to that in the bare-fuel test, but $^{129}I$ released in the hole-defects test was not significantly greater than in the undefected test.

10. Comparison of $^{14}C$ solution activity data measured in the sealed Series 3 tests to that measured in the unsealed Series 2 tests indicated that most of the $^{14}C$ released in the Series 2 tests was probably lost to the atmosphere as $^{14}CO_2$. The TP fuel appeared to have a much greater $^{14}C$ inventory (or gap inventory) than did the HBR fuel on which fuel and cladding $^{14}C$ inventory was radiochemically determined.

11. Long-term release rates for soluble nuclides are uncertain. The relative contributions of fuel matrix phase dissolution, versus preferential release from locations such as grain boundaries where soluble nuclides may be concentrated, was not determined. Preferential release would likely decrease as the inventory of soluble nuclides on exposed grain boundaries is depleted. However, there is reason to suspect that accelerated dissolution of soluble nuclides may eventually occur as a result of degradation of the fuel by oxidation in the repository air atmosphere.

12. A vessel corrosion anomaly occurred during Cycle 1 of the 85°C HBR bare-fuel test. The most significant effects associated with the apparent vessel corrosion were: 1) uranium concentration dropped to about 10 ppb, and 2) $^{99}Tc$ activity dropped to less than detectable. These effects are attributed to removal of uranium and technetium by coprecipitation with or sorption on iron-bearing precipitates, or to reduction of the soluble $UO_2^{+2}$ and $NpO_2$ species as a result of redox coupling with $Fe^0$ to $Fe^{+2}/Fe^{+3}$ reactions.

13. Calcium, magnesium, silicon, and $HCO_3$ precipitated from solution during all 85°C tests cycles, while the chemistry of the starting J-13 well water remained essentially unchanged during the 25°C test. In addition to the calcium-uranium-silicate phases observed in the two 85°C bare-fuel tests, scale formation was observed at the waterline in all of the 85°C tests. The SEM-EDX examinations suggest that calcite, $SiO_2$ (possibly as a gel), and possibly dolomite were formed during the 85°C tests. A portion of the released $^{14}C$ is likely to be incorporated in the carbonate phases. A portion of the released $^{90}Sr$ is also likely to be incorporated in secondary phases, possibly as a partial substitute for calcium.

Summary of "Semi-static" Unsaturated Tests and Geochemical Modeling

The following summary was extracted from Wilson and Bruton (1990c). The full text of that paper is attached to this section as Addendum 1. Laboratory testing and geochemical simulation of the dissolution of spent fuel under conditions selected for relevance to the proposed Yucca Mountain repository have resulted in the following conclusions.

1. Radionuclides of interest in spent fuel appear to fall into three categories of potential release mechanisms: 1) radionuclides whose release appears to be controlled by concentration-limiting mechanisms, 2) more highly soluble radionuclides, and 3) radionuclides that are released in the vapor phase (principally C-14).

2. The principal radionuclides whose releases appear to be controlled by concentration-limiting mechanisms are the actinides U, Np, Pu, Am and Cm. Steady-state concentrations measured for these actinide elements are at least three orders of magnitude lower than those required to meet NRC release limits based on conservative estimates of water fluxes through the repository. This result is of particular significance because isotopes of Pu and Am account for about 98% of the activity in spent fuel at 1000 years. However, results from geochemical modeling suggest that steady-state concentrations may vary significantly with time because of changes in solution composition and the identity of precipitating phases.

3. Good agreement between measured and predicted concentrations was obtained for Np based on equilibration with $NpO_2$ at 25°C when the oxygen fugacity in the simulation was set at $10^{-12}$ bars. A broad range of solubilities that bracketed the measured values were predicted for Pu depending upon the assumed oxygen fugacity and solubility-controlling phase. Measured Am concentrations were less than predicted based on data for equilibration with $Am(OH)CO_3$ and $Am(OH)_3$.

4. Dissolution rates for soluble radionuclides ($^{137}Cs$, $^{90}Sr$, $^{99}Tc$ and $^{129}I$) exceeding $10^{-5}$ of specimen inventory per year were measured during the laboratory tests. The implications of these data relative to long-term release of soluble radionuclides from a failed waste package are uncertain. The degree to which these radionuclides were preferentially released from grain boundaries where they may have concentrated during irradiation was not determined. Preferential release could be expected to provide a lesser contribution overtime as exposed grain boundary inventories are depleted. However, physical degradation of the fuel over time from exposure to the oxidizing repository environment may result in accelerated release of soluble nuclides.

5. Additional work is required to identify solid phases that control actinide concentrations, and to acquire reliable thermodynamic data on these phases for use in geochemical modeling. In this regard, identification of any stable suspended phases that can be transported by water movement is also important. In addition, there is a need for a better understanding of the potential release of soluble and volatile radionuclides, which may initially depend on preferential release from gap and grain boundary inventories, but may ultimately depend on the rate of fuel degradation by oxidation or other processes in the postcontainment repository environment.

## 2.1.3.5.3 FLOWTHROUGH DISSOLUTION TESTS

The purpose of the work reported here is to examine the systematic effect of temperature and important water chemistry variables on the dissolution rates of the $UO_2$ matrix phase in both unirradiated $UO_2$ and spent fuel. The dissolution rates of the higher oxidation states of uranium, $U_4O_{9+x}$, $U_3O_8$ and $UO_3 \cdot xH_2O$ are also reported, because of their likely presence in spent fuel placed in a repository. Unirradiated $UO_{2+x}$ represents reactor fuel with no burnup. The data sets, obtained at equivalent conditions allow a direct comparison of $UO_{2+x}$ and spent fuel dissolution rates and provide insight into the effect of fuel burnup. Additional data at higher spent fuel burnup are needed to model the effect of burnup over the range of spent fuel inventory.

The exact chemistry of groundwater in an underground repository is not certain, but groundwater has typical constituents, such as carbonates, sulfates, chlorides, silicates, and calcium. Water taken from wells near Yucca Mountain, contains all of these ions and has a pH near 8. Of the anions commonly found in groundwater, carbonate is considered to be the most aggressive towards $UO_2$ and, as such, is a conservative surrogate for all anions in groundwater. The data obtained from the tests described here can be used to: 1) identify important parameters that control the dissolution rates of the $UO_2$ matrix phase of spent fuel, 2) estimate bounding values for $UO_2$ and spent fuel matrix dissolution rates, and 3) develop a release model for radionuclides from spent fuel that will be used in waste package design and in performance assessment.

The intrinsic dissolution rates of $UO_{2+x}$ and spent fuel were determined by using a single pass flow-through method that was used successfully in the study of the dissolution kinetics of glass and other minerals. The advantage of the single pass flow-through technique is that flow rates and specimen size can be controlled so that the $UO_2$ dissolves under conditions that are far from solution saturation (no precipitation of dissolved products). Under such conditions, the steady-state dissolution rates are directly proportional to the effective surface area of the specimen. Thus, the dependence of $UO_2$ dissolution kinetics on pH, temperature, oxygen and carbonate/bicarbonate concentrations can be evaluated.

A set of experiments was selected to examine systematically the effects of temperature (25-75°C), dissolved oxygen (0.002-0.2 atm overpressure), pH (8-10) and carbonate concentrations (0.2-20 millimol/L) on $UO_2$ and spent fuel dissolution (Steward and Gray 1994). Similar sets of experiments at atmospheric oxygen partial pressure were conducted on $U_3O_8$ and $UO_3 \cdot xH_2O$ to measure the effect of higher oxidation states on dissolution. The high temperature in all experiments was limited to 75°C, because temperatures nearer to 100°C induce experimental difficulties in an aqueous, flowthrough system. The carbonate concentrations bracketed the typical groundwater concentration of 1 millimol/L. The oxygen pressure represented the atmospheric value and down two orders of magnitude to a minimally oxidizing atmosphere. The pH covered a value typical of groundwaters (pH=8) to very alkaline conditions. In the basic region carbon dioxide dissolved in water, $CO_2$ (aq), occurs mostly as carbonate/bicarbonate species. Therefore, carbonate/bicarbonate concentrations were fixed by adding solid carbonates/bicarbonates to those basic buffer solutions, and the partial pressure of $CO_2$ in the gas phase above them will be kept at the values calculated for stability. The spent fuel used in the PNL tests was ATM-103, a PWR fuel with a burnup of 33 MWd/kgM and a fission gas release of 0.25%. The $UO_2$ specimens used at LLNL were about 1 cm across and consisted of large crystallites containing dislocation substructures, i.e., low-angle grain boundaries.

Table 2.1.3.5-3 provides a list of the spent fuels used in the flow-through dissolution and other tests.

**Table 2.1.3.5-3. Spent Fuel Test Materials**

| Reactor Type | Fuel | Rod | Peak Burnup (MWd/kgM) | Fission Gas Release (%) |
|---|---|---|---|---|
| PWR | ATM-103 | MLA-098 | 30 | 0.25 |
| PWR | ATM-104 | MKP-109 | 44 | 1.1 |
| BWR | ATM-105 | ADD-2974 | 31 | 0.59 |
| BWR | ATM-105 | ADD-2966 | 34 | 7.9 |
| PWR | ATM-106 | NBD-095 | 43 | 7.4 |
| PWR | ATM-106 | NBD-107 | 46 | 11 |
| PWR | ATM-131 | NBD-131 | 50 | 18 |

Flowthrough Test Results

The results of the combined uranium dioxide and ATM-103 spent fuel test matrices are given in Table 2.1.3.5-4. Two different averages of the ATM-103 spent fuel and $UO_2$ data were calculated. The first was for 20% oxygen (air) and the second was for all tests where the conditions were nominally identical. For both averages, the $UO_2$ rates were about three times higher than the spent fuel rates. This is not a large difference for this type of test and is comparable to that observed when the two laboratories tested separate portions of the same batch of $UO_2$ powder. Thus, there may be no real difference between the spent fuel and the $UO_2$, except for the clear difference in the way the two materials responded to changes in oxygen concentration. Aside from oxygen concentration, both spent fuel and $UO_2$ dissolution rates were most dependent on temperature followed by a lesser dependence on carbonate concentration. Changes in pH had the least effect on the dissolution rates of both materials.

Additional spent fuel data are available for specific fuels and conditions (Gray and Wilson 1995, Gray 1996). These seven dissolution rates of unoxidized higher-burnup fuels are listed in Table 2.1.3.5-4a. The combined 49 dissolution rates from Tables 2.1.3.5-4 and 4a are used in the second Butler-Volmer model of Section 3.4.2; the first Butler-Volmer model developed earlier uses only the data from 42 runs in

Table 2.1.3.5-4, plus the mid-setting run for ATM-105 at 50°C, pH of 9, 2 x $10^{-3}$ M total carbonate and atmospheric oxygen.

The dependence of $UO_{2+x}$ dissolution kinetics on pH, temperature, time and carbon dioxide/carbonate/bicarbonate concentrations were also investigated. All experiments in this higher oxide test series were run at 20% oxygen buffer solution overpressure or 8 ppm dissolved oxygen. The flow-through tests were carried out in basic buffer solutions (pH of 8 to 10). The chemical composition of the solutions provide concentrations and dissolution rate data useful in developing kinetic models for $UO_2$ matrix dissolution of spent fuel and for use in the waste package design. The intrinsic dissolution rate obtained from these data is expected to be an upper bound dissolution response for high pH water chemistries. Again in order to test for nonlinear effects, experiments at three different values of each quantitative or continuous variable are required. Tests were done at three temperatures (25°, 50° and 75°C) three carbonate/bicarbonate concentrations ($2x10^{-4}$ - $2x10^{-2}$ mol/L) and three pH's (8, 9, 10) using an arbitrary flow rate (>100 mL/day) for the two compounds, $U_3O_8$ and $UO_3 \cdot xH_2O$.

**Table 2.1.3.5-4. Test Parameters and Results for Spent Fuel and $UO_2$ Dissolution T**

| Run No. | Temp. (°C) | Carbonate[b] (mmol/L) | Oxygen[c] % | pH[d] | U Dissolution Rate ($mg/m^2 \cdot day$) Spent Fuel (ATM-103) | $UO_2$ |
|---|---|---|---|---|---|---|
| 1 | 50 | 2 | 20 | 9.0 | 6.34 | |
| 2 | 50 | 2 | 20 | 9.0 | 7.05 | |
| 3 | 50 | 2 | 20 | 9.0 | 5.07 | |
| 4 | 22/25 | 20 | 20 | 8.0/8.7 | 3.45 | 2.42 |
| 5 | 74/75 | 20 | 20 | 10.0/10.3 | 14.2 | 77.4 |
| 6 | 74/75 | 0.2 | 20 | 8.0/9.1 | 8.60 | 10.9 |
| 7 | 21/25 | 0.2 | 20 | 10.0/9.0 | 0.63 | 2.55 |
| 8 | 22/25 | 20 | 20 | 9.0/9.4 | 2.83 | 6.72 |
| 9 | 22/25 | 2 | 20 | 10.0/9.3 | 2.04 | 9.34 |
| 10 | 27/26 | 0.2 | 2 | 8.0/7.8 | 1.79 | 0.12 |
| 11 | 78/75 | 0.2 | 2 | 10.0/9.7 | 1.49 | 9.21 |
| 12 | 25/26 | 20 | 2 | 10.0/10.1 | 2.05 | 1.87 |
| 13 | 77/75 | 20 | 2 | 8.0/8.5 | 2.89 | 5.11 |
| 14 | 23/25 | 20 | 0.3/0.2 | 8.0/8.0 | 2.83 | 0.22 |
| 15 | 74/75 | 20 | 0.3/0.2 | 10.0/9.8 | 0.69 | 5.61 |
| 16 | 78/75 | 0.2 | 0.3/0.2 | 8.0/8.7 | 1.98 | 0.51 |
| 17 | 19/26 | 0.2 | 0.3/0.2 | 10.0/9.3 | 0.51 | 0.23 |
| 18 | 50/50 | 20 | 0.3/0.2 | 10.0/9.9 | 1.04 | 4.60 |
| 19 | 21/26 | 2 | 0.3/0.2 | 9.0/9.0 | 1.87 | 1.52 |
| 20 | 75 | 20 | 2 | 10.0 | 4.75 | |
| 21 | 50 | 2 | 2 | 8.9 | | 12.3 |
| 22 | 50 | 2 | 2 | 8.8 | | 7.96 |
| 23 | 50 | 2 | 2 | 8.9 | | 10.4 |
| 24 | 75 | 0.2 | 20 | 9.5 | | 6.48 |
| 25 | 75 | 2 | 20 | 9.6 | | 23.3 |
| 26 | 75 | 20 | 20 | 8.5 | | 54.0 |
| Average | Runs 4-9 | | | | 5.29 | 18.2 |
| Average | Runs 4-19 | | | | 3.08 | 8.57 |

(a) Numbers separated by a "/" are data for spent fuel and $UO_2$ respectively (SF/$UO_2$)

(b) Made up using appropriate amounts of $Na_2CO_3$ and $NaHCO_3$

(c) Percent of oxygen in sparge gas

(d) Measured at room temperature. For spent fuel, the measured values were within $\pm 0.1$ unit of the nominal values listed.

**Table 2.1.3.5-4a. Additional Spent Fuel Flow-Through Dissolution Tests.**

| | | | Intrinsic Dissolution Rates [mg/(m$^2$-day)] | | | | |
|---|---|---|---|---|---|---|---|
| | | | pH=8 | | pH=8 | | pH=9 |
| | | | 2 x 10$^{-2}$ M | | 2 x 10$^{-4}$ M | | 2 x 10$^{-4}$ M |
| | | | Total Carbonate | | Total Carbonate | | Total Carbonate |
| Fuel | Rod | Burnup (MWd/kgM) | 25°C | 75°C | 25°C | 75°C | 50°C |
| ATM-104 | MKP-109 | 44 | 3.4 | | | | |
| ATM-105 | ADD-2974 | 31 | 3.5 | 7.8 | 2.7 | 11 | 7 |
| ATM-106 | NBD-131 | 50 | 1.5 | | | | |

Dehydrated schoepite, $UO_3 \cdot xH_2O$, is used in the $UO_3$ runs. It is easy to produce and is more stable than either the dihydrate or anhydrous form of uranium trioxide. Approximately 20 grams of $UO_3 \cdot xH_2O$ were prepared via an aqueous hydrolysis of uranyl acetate, $UO_2(Ac)_2$, a procedure that took place over several days. The $U_3O_8$ in use is NBS Standard Reference Material 750b. It can also be produced by heating the dehydrated schoepite in air. Both $U_3O_8$ and $UO_3 \cdot xH_2O$ samples were powders because of the synthetic routes available for each. The $U_3O_8$ powders were National Bureau of Standards (NBS or NIST) Standard Reference Material (SRM) 750(b). $U_3O_8$ is the most stable of the uranium oxides and is easily produced by the well known method of heating a uranium compound, $UO_2$ in this case, to several hundred degrees centigrade in air. Surface areas of both materials were measured via the traditional Brunauer-Emmett-Teller (BET) method using xenon gas. The resulting surface area for the $U_3O_8$ is 0.18±0.02 m$^2$/g and 0.31± 0.04 m$^2$/g for the $UO_3 \cdot xH_2O$. Particle size distributions were also determined by means of sedimentation techniques. The median particle size for the $U_3O_8$ powder was 2.1 μm with a 25-75 percentile range of 1.0 to 2.8 μm. The median particle size for the $UO_3 \cdot xH_2O$ powder was 4.1 μm with a 25-75 percentile range of 2.5 to 5.5 μm.

Table 2.1.3.5-5 lists the uranium dissolution rates for the three oxides, $UO_2$, $U_3O_8$ and $UO_3 \cdot xH_2O$, that were measured at LLNL under atmospheric oxygen conditions. The two new room-temperature $UO_2$ results were measured at a pH of 10 and 2 x 10$^{-4}$ molar total carbonate and a pH of 10 at 2 x 10$^{-2}$ molar total carbonate. These were recently acquired so that there would be a full set of eight measurements at the extreme conditions (a full-factorial linear experimental design) for each oxide. Previously obtained results for spent fuel (ATM-103) are listed at equivalent conditions. To facilitate easier comparisons of the dissolution rates and variable effects, the results for the eight experimental conditions at the high and low values of each variable are grouped together at the beginning of the table (Part 1). They are grouped first by pH, then by carbonate concentration and finally by temperature.

The results at intermediate conditions are listed last as Part 2 in Table 4, using the same grouping scheme.

As shown in Table 2.1.3.5-5, Part 1 the oxide state has by far the strongest effect on the uranium dissolution rate. The rate increases significantly in going from $UO_2$ to $U_3O_8$ and dramatically from $U_3O_8$ to $UO_3 \cdot xH_2O$. Increasing carbonate concentrations increase the dissolution rates of $U_3O_8$ and $UO_3 \cdot xH_2O$, as shown previously with $UO_2$. An increase in $U_3O_8$ dissolution rate with increasing temperature was seen as well. A similar temperature effect on $UO_3 \cdot xH_2O$ is not apparent, which may be due to the rapid $UO_3 \cdot xH_2O$ dissolution. Raising the temperature to 75°C from room temperature increases the dissolution rate by a factor of 2 to 4 for the two higher oxides. As with the $UO_2$ results, alkaline pH does not have a significant role in changing the dissolution rate of the higher oxides. However, the detailed dependence on temperature and carbonate concentrations is not visually well shown. Since pH shows little correlation, a surface plot for dissolution rate in three dimensions would better show the effects of carbonate concentration and temperature.

The data in Table 2.1.3.5-5 indicate that with the higher oxides, unlike $UO_2$, carbonate seems to affect the dissolution rate to a greater extent than does temperature. The enhancement is particularly strong at the highest carbonate concentration.

Because $U_3O_8$ has both U(IV) and U(VI) valence states, its dissolution rates might be expected to be between that of $UO_2$ and $UO_3 \cdot xH_2O$, particularly as carbonate concentrations increase. That does not seem to be the case with the present data. The data indicate that alkaline pH is the least significant factor in dissolution of spent fuel or any of the uranium oxides under the alkaline conditions of these experiments. Changes in alkaline pH produce almost random changes in dissolution rates in this and previous data sets.

**Table 2.1.3.5-5, Part 1. Comparison of Dissolution Rates at Bounding Conditions**

| pH | Carbonate | Oxygen | Temp | | Dissolution Rate (mgU/($m^2$·day)) | | |
|---|---|---|---|---|---|---|---|
| | (mol/L) | (atm) | deg C | ATM-103 Spent Fuel | $UO_2$ | $U_3O_8$ | $UO_3 \cdot xH_2O$ |
| 8 | 0.0002 | 0.2 | 25 | | 3.87 | ~5 | ~100 |
| 8 | 0.0002 | 0.2 | 50 | | 5.4 | | |
| 8 | 0.0002 | 0.2 | 75 | 8.6 | 10.9 | ~6 | >200 |
| 8 | 0.02 | 0.2 | 25 | 3.45 | 2.42 | 18.8 | ~700 |
| 8 | 0.02 | 0.2 | 50 | | 38.3 | | |
| 8 | 0.02 | 0.2 | 75 | | 54 | ~150 | >1500 |
| 10 | 0.0002 | 0.2 | 25 | 0.63 | 2.55 | 0.8 | >100 |
| 10 | 0.0002 | 0.2 | 50 | | 3.1 | | |
| 10 | 0.0002 | 0.2 | 75 | | 6.48 | ~3 | >150 |
| 10 | 0.02 | 0.2 | 25 | | 20.1 | 21.1 | ~200 |
| 10 | 0.02 | 0.2 | 50 | | 25.8 | | |
| 10 | 0.02 | 0.2 | 75 | 14.2 | 77.4 | ~200 | >1000 |

**Table 2.1.3.5-5, Part 2. Comparison of Dissolution Rates at Intermediate Conditions**

| pH | Carbonate | Oxygen | Temp | | Dissolution Rate (mgU/($m^2$·day)) | | |
|---|---|---|---|---|---|---|---|
| | (mol/L) | (atm) | deg C | ATM-103 Spent Fuel | $UO_2$ | $U_3O_8$ | $UO_3 \cdot xH_2O$ |
| 8 | 0.002 | 0.2 | 25 | | | ~10 | |
| 8 | 0.002 | 0.2 | 50 | | | ~10 | |
| 9 | 0.0002 | 0.2 | 25 | | | 1.26 | |
| 9 | 0.0002 | 0.2 | 75 | | | ~4 | |
| 9 | 0.002 | 0.2 | 25 | | | | ~120 |
| 9 | 0.002 | 0.2 | 50 | 6.1 | 11.7 | | |
| 9 | 0.002 | 0.2 | 75 | | 23.3 | | >20 |
| 9 | 0.02 | 0.2 | 25 | 2.83 | 6.72 | 8.33 | >1500 |
| 9 | 0.02 | 0.2 | 50 | | | >100 | |
| 10 | 0.002 | 0.2 | 25 | 2.04 | 9.34 | | |

Dissolution Rates of Oxidized Spent Fuel and Additional Tests With Unirradiated Uranium Oxides

Uranium dissolution rates were measured on crushed unirradiated $UO_2$ fuel pellet samples under oxidizing conditions using the flow-through test method (Wilson and Gray 1990). Water compositions included J-13 well water, deionized distilled water (DIW), and variations on the J-13 water composition selected to measure the effects of various J-13 water components on $UO_2$ dissolution rates. Dissolution rates at 25°C in air-equilibrated DIW were 1-2 mgU/($m^2$·day)). Calcium (15 µg/ml as $CaCl_2$ and $CaNO_3$) and silicon (30 µg/ml as silicic acid) were sequentially added to the DIW, resulting in an order of magnitude decrease in uranium dissolution rate. Adding $NaHCO_3$ in concentrations similar to J-13 water (170 µg/ml) to this calcium and silicon containing DIW increased the uranium dissolution rate by almost two orders of magnitude.

Results from flow-through dissolution tests with oxidized specimens of spent fuel and unirradiated $U_3O_7$ and $U_3O_8$ have been published (Gray and Thomas 1992; Gray, Thomas and Einziger 1993; and Gray and Thomas 1994). Therefore, only highlights are discussed here together with some details that were not included in these publications (Gray and Wilson 1995).

Dissolution rates of spent fuels oxidized to $U_4O_{9+x}$ currently have been measured for three spent fuels, ATM-104, ATM-105 and ATM-106. The surface area normalized dissolution rate of oxidized fuel grains was little or no higher than unoxidized ($UO_2$) grains for ATM-105. Oxidized ATM-106 fuel grains dissolved somewhat faster than unoxidized grains, but still the difference was a factor of only about five.

Note that the test conditions for ATM-105 were different from those used with the ATM-104 and ATM-106 fuels (see Table 2.1.3.5-6). This precludes a direct comparison between ATM-105 and the other two fuels. However, the purpose of the tests in each case was to compare results for oxidized versus unoxidized specimens, not for comparison between different fuels. The tests with ATM-105 were conducted first, and a decision was made after that to change the conditions for future tests. This test condition ($2 \times 10^{-2}$ M total carbonate, pH =8, 25°C, atmospheric oxygen partial pressure), which will be included in most future testing to allow a wider variety of direct comparisons between different fuels, was used for the oxidized and unoxidized specimens of ATM-104 and ATM-106 fuels.

Oxidation has the potential to change spent fuel dissolution rates in two ways. First, it could change the intrinsic dissolution rates. Second, it could increase the dissolution rate of fuel particles by making the grain boundaries more accessible to the water thereby increasing the effective surface area.

Table 2.1.3.5-6 shows that the intrinsic dissolution rates of ATM-104 and ATM-105 (data obtained using grain specimens) were not significantly affected by oxidation, but there was a modest increase in the intrinsic dissolution rate of ATM-106 fuel grains. Secondly, oxidation left the dissolution rate of ATM-105 particles unchanged, which implies that the depth of water penetration into the grain boundaries was unchanged by the oxidation.

In contrast to the ATM-105 particles, oxidation had a marked effect on the dissolution rates of ATM-104 and ATM-106 particles. This effect can be attributed to opening of the grain boundaries by the oxidation, which allows greater water penetration thereby increasing the effective surface area available for reaction with the water. So great was this effect with ATM-104 that the water appears to have penetrated the entire volume of grain boundaries throughout the particles. This is evident from the estimated depth of water penetration (~100 grain layers) multiplied by the grain size (~12 μm), which leads to a penetration depth that is well over half the particle diameters (700 to 1700 μm).

Because replicate tests have not been run, it is not possible to say whether the three different fuels in Table 2.1.3.5-6 really respond differently to oxidation and subsequent reaction with water or if the observed differences were simply sample-to-sample variations. However, the data do suggest that oxidation up to the $U_4O_{9+x}$ stage does not have a large effect on intrinsic dissolution rates (the largest increase was a factor of <6). However, data for some of the particle specimens suggest that this degree of oxidation may markedly increase dissolution rates of relatively intact fuel rods by opening the grain boundaries and thereby increasing the effective surface area that is available for contact by water. From a disposal viewpoint, this is the more important consideration.

**Table 2.1.3.5-6. Dissolution Rate ($mg \cdot m^{-2} \cdot d^{-1}$) and Estimated Grain Boundary Penetration of Unoxidized ($UO_2$) and Oxidized ($U_4O_{9+x}$) Spent Fuel**

| | | Unoxidized | | | Oxidized | | |
|---|---|---|---|---|---|---|---|
| Fuel | Rod | Grains | Particles | GBP[a] | Grains | Particles | GBP[a] |
| ATM-104[b] | MKP-109 | 3.4 | 33 | 4-6 | 3.5 | 166 | ~100 |
| ATM-106[b] | NBD-131 | 1.5 | 25 | 6-9 | 8.2 | 241 | 12-18 |
| ATM-105[c] | ADD-2974 | 6.6 | 25 | 2-3 | 7.4 | 28 | 2-3 |

(a) Grain Boundary Penetration. Estimate of depth of water penetration into the grain boundaries (number of grain layers)

(b) $2 \times 10^{-2}$ M total carbonate, pH =8, 25°C, atmospheric oxygen partial pressure

(c) $2 \times 10^{-3}$ M total carbonate, pH =9, 50°C, atmospheric oxygen partial pressure

When ATM-106 fuel was oxidized to $U_3O_8$, its surface area normalized dissolution rate was about 10 times faster than unoxidized ATM-106 fuel grains and about twice as fast as ATM-106 fuel grains oxidized to $U_4O_{9+x}$. A more important effect of oxidation to $U_3O_8$ was the very large increase in surface area compared to the particles used to prepare the $U_3O_8$. This resulted in a fractional dissolution rate (rate per unit specimen weight) of $U_3O_8$ equal to 150 times that of the unoxidized particles.

At atmospheric $O_2$ overpressure, the intrinsic dissolution rate of unirradiated $U_3O_7$ (~3 $mgU/(m^2 \cdot day)$) was similar to $UO_2$ (~2.5 $mgU/(m^2 \cdot day)$) and the intrinsic dissolution rate of unirradiated $U_3O_8$ (~10-15 $mgU/(m^2 \cdot day)$) was about three to five times that of $UO_2$. At an $O_2$ overpressure of 0.003 atm, the intrinsic dissolution rate of the $U_3O_7$ was two to three times that of $UO_2$ (0.5-1 $mgU/(m^2 \cdot day)$). These estimates are based on single experiments with each oxide at each condition.

In summary, for each test conducted with oxidized spent fuel or unirradiated $U_3O_7$ or $U_3O_8$, the intrinsic dissolution rate of the oxidized material was only moderately higher than the unoxidized ($UO_2$) material. The largest difference was a factor of 10 with spent fuel $U_3O_8$. This difference seems relatively small when it is considered that the surface of $UO_2$ must first oxidize to a stoichiometry equivalent to approximately $UO_{2.33}$ before significant dissolution of U, as U(VI) species, can occur.

These observations suggest that initial surface oxidation is not involved in a rate-limiting step of the $UO_2$ oxidation/dissolution mechanism.

A major reason for conducting dissolution tests with spent fuel oxidized to $U_3O_8$ was to determine whether the inter- and intra-granular cracks produced by the oxidation would lead to high initial dissolution rates of soluble radionuclides. Therefore, 100% of the test-column effluent was collected and analyzed for each of the first two days. During the first day (29 h), 16.2% of the total $^{137}Cs$ inventory dissolved compared with 4.5% of the U; thus the excess of $^{137}Cs$ over U was about 12%, which represents the amount exposed by oxidation-induced cracking and grain-boundary opening. Nearly congruent dissolution of $^{137}Cs$ and U was observed during the second and subsequent days.

Because the fuel particles were washed before they were oxidized to $U_3O_8$, the $^{137}Cs$ associated with the gap inventory would have been removed. Also, the $^{137}Cs$ inventory associated with grain boundaries of this fuel was only about 1% of the total $^{137}Cs$ inventory. Therefore, of the 12% excess of $^{137}Cs$ over U cited above, only 1% could have come from oxidation-induced opening of the grain boundaries. The remaining 11% had to originate from oxidation-induced cracking of the grain interiors. This confirms speculation that oxidation to $U_3O_8$ might expose a relatively large fraction of the $^{137}Cs$ inventory to water where it could be readily dissolved, at least for this one type of spent fuel (ATM-106).

### 2.1.3.5.4 UNSATURATED DISSOLUTION TESTS

Part of this section summarizes work in Bates et al. 1995. In scenarios for the potential Yucca Mountain repository, it is assumed that the cladding has failed and water as vapor or liquid contacts the fuel. Drip tests that simulate the unsaturated and oxidizing conditions expected at Yucca Mountain are in progress to evaluate the long-term behavior of spent nuclear fuel. The purpose of the experiments is to determine if the rate of fuel alteration affects the release rate[2] of different radionuclides under unsaturated conditions. The results from the drip tests are used to monitor the reaction rate of the fuel, the corresponding release rates for individual radionuclides, as well as the solution chemistry. The information from these tests can be used to estimate the magnitude of the potential radionuclide source term at the exterior of the fuel cladding, and the changes that can be expected in water chemistry due to groundwater interaction with the spent fuel.

---

[2] In these unsaturated tests radionuclide release means the quantity of those elements that go into solution as dissolved or colloidal species or precipitate on the container walls. The quantity of sample that initially dissolves and reprecipitates on the sample or sampleholders is not measured or included in the mass release totals. Therefore, estimates of dissolution rates cannot be directly compared to flowthrough dissolution rates.

The reaction of $UO_2$ and spent nuclear fuel samples was examined in unsaturated drip tests that simulate an environment that may be expected for spent fuel in the unsaturated/oxidizing environment of the potential Yucca Mountain nuclear waste repository. The reaction of both $UO_2$ and spent fuel occurs rapidly in these tests, resulting in the formation of alteration phases that replicate those observed during the oxidative dissolution of uraninite in natural geologic systems. Overall reaction pathways for both $UO_2$ and spent fuel appear to be controlled by a combination of sample corrosion, precipitation kinetics of alteration phases, and leachant composition.

$UO_2$ Reactions Through 10 Years of Testing

The present unsaturated drip tests with $UO_2$ using EJ-13 water at 90°C are being conducted, because direct testing of spent fuel is difficult due to its high level of radioactivity, unirradiated $UO_2$ is being used as a surrogate for spent fuel. While these experiments are not completely analogous to spent fuel behavior, the reaction processes occurring during the corrosion of spent fuel and $UO_2$ may be similar since spent fuel contains >95% $UO_2$. Therefore, the gross processes observed in the $UO_2$ experiments should be relevant to spent fuel behavior, especially with respect to the identification of secondary alteration products and modes of waste form degradation. More specifically, these tests are designed to examine the dissolution behavior of the $UO_2$ pellets, identify long-term alteration mineral paragenetic trends, describe parameters that control the release of uranium from the $UO_2$ pellets, and serve as a pilot study for similar tests with spent nuclear fuel.

Uranium release from the $UO_2$ samples was rapid from one to two years of testing, followed by relatively low rates of release over the two- to ten-year period. The rapid release period could be correlated with an episode of preferential corrosion along $UO_2$ grain boundaries and the subsequent spallation of micrometer- to submicrometer-sized $UO_{2+x}$ particles (where $0 \geq \chi \leq 1$) from the sample surfaces. Electron microscopy and optical examinations of the altered samples revealed the presence of a reaction front that penetrated into the samples an average of two-to-four grains (~10 to 20 μm) ahead of the exposed external sample surface, but varied from regions with little visible corrosion, to regions where penetration occurred to a depth of approximately ten grains. This corrosion occurred preferentially along the grain boundaries between the original press-sintered granules comprising the $UO_2$ pellets (Fig. 2.1.3.5-1a). The formation of a dense mat of alteration phases in the longer-term tests enveloped the loosened $UO_2$ grains (Fig. 2.1.3.5-1b), resulting in a reduction of particulate spallation and a lowering of uranium release rates.

Unfiltered uranium release rates from the two-to ten year period are variable, but were generally between 0.1 and 0.3 $mg/m^2 \cdot day$. An analysis of the size-fractioned release patterns during this period indicates that the majority (86 to 97%) of the

released uranium was sorbed or precipitated on the walls of the stainless steel test vessel and the Teflon support stand. Between 1 to 12% was present as >5 nm sized particles suspended in the leachate, whereas less than 2% of the total uranium could be attributed to components that passed through a filter with a 5-nm pore-size opening. This latter fraction suggests a uranium concentration of $4 \times 10^{-6}$ M for the leachate collected from the bottom of the test vessel.

A cross-section examination of the samples indicated that the vast majority of the uranium released from the dissolving samples was deposited on the surface of the $UO_2$ pellets and Zircaloy cladding as alteration phases. The quantity of uranium that was incorporated in these phases was calculated by determining the volume of precipitated material on the sample surface, proportion of each respective alteration phase present, the molar proportion of uranium contained in each phase, and multiplying the calculated volume of each respective phase present by its respective density. Preliminary calculations for sample PMP8U-2 (Table 2.1.3.5-7), reacted for eight years, indicate that ~80 mg of uranium was incorporated into the alteration phases deposited on the sample or Zircaloy surfaces, an amount that far exceeds the 5 mg that was released from the sample-Zircaloy assembly (as recovered in the acid strip component). An additional ~780 mg of uranium remained *in situ* as undissolved $UO_{2+x}$ cores that had undergone some corrosion along their grain boundaries. The initial $UO_2$ pellet weights prior to testing were 29,166 mg (25,709 mg of uranium).

**Table 2.1.3.5-7. Fractional Distribution of Uranium from Unsaturated Drip Tests with $UO_2$ and Spent Fuel (Values in mg and total percent in parentheses).**

| Test | Acid Strip | Alteration Phases | Grain Boundary Corroded | Unaffected Region | Initial Sample Weight |
|---|---|---|---|---|---|
| 8 Year $UO_2$ | 5.0 (0.02%) | 80 (0.3%) | 780 (3.0%) | 24,844 (96.6%) | 25,709 |
| Spent Fuel[a] | ND[c] | 180 (2.3%) | All Visible | None | 8,000 |
| Spent Fuel[b] | 250 (Acid Strip + Alteration Phases) (3.1%) | | ND | ND | 8,000 |

[a]Fractions determined from measured cross-sections of alteration layers.

[b]Fractions determined from Tc release.

[c]ND = not determined.

The $UO_2$ sample reaction trends closely replicate those observed in natural uraninite deposits, such as the Nopal I deposit in Mexico. Both the natural and experimental systems display a paragenetic sequence of mineral phase formation that is characterized by the following trend: $UO_2 \Rightarrow$ uranyl oxide hydrates $\Rightarrow$ alkali- and alkaline-earth uranyl oxide hydrates $\Rightarrow$ uranyl silicates $\Rightarrow$ alkali- and alkaline-earth uranyl silicates + palygorskite clay (Table 2.1.3.5-8).

**Table 2.1.3.5-8. Summary of $UO_2$ Alteration Phases**

| | |
|---|---|
| Uranyl-Oxide Hydrates | |
| Schoepite (meta-schoepite) | $UO_3 \cdot nH_2O$ ($n < 2$) |
| Dehydrated Schoepite | $UO_3 \cdot (0.8\text{-}1.0H_2O)$ |
| Compreignacite | $(Na,K)_2[(UO_2)_6O_4(OH)_6] \cdot 8H_2O$ |
| Becquerelite | $Ca[(UO_2)_6O_4(OH)_6] \cdot 8H_2O$ |
| Uranyl Silicate Hydrate | |
| Soddyite | $(UO_2)_2SiO_4 \cdot 2H_2O$ |
| Uranyl Alkaline Silicate Hydrates | |
| Uranophane | $Ca(UO_2)(SiO_3)(OH)_2 \cdot 5H_2O$ |
| Boltwoodite | $K_2(UO_2)_2(SiO_4)_2(H_3O)_2 \cdot H_2O$ |
| Na-Boltwoodite | $(Na,K)(UO_2)(SiO_4)(H_3O) \cdot H_2O$ |
| Sklodowskite | $Mg(UO_2)_2(SiO_4)_2(H_3O)_2 \cdot 2H_2O$ |
| Non-Uranyl Phases | |
| Palygorskite | $(Mg,Al_{0.12\text{-}0.66})_5(Si,Al_{0.120.66})_8O_{20}(OH)_5 \cdot 4H_2O$ |
| Fe-Oxides | |
| Ti-Oxides | |
| Amorphouse Silica | |

The alkali- and alkaline-earth uranyl silicates represent the long-term solubility-limiting phases for uranium in the $UO_2$ tests and the natural uranium deposits at Nopal. This similarity suggests that the present experiments and the natural analogue reactions may simulate the long-term reaction progress of spent $UO_2$ fuel following disposal at the proposed Yucca Mountain repository.

Spent Nuclear Fuel reactions After 3.7 Years

Oxidation/dissolution of the spent fuel occurred rapidly in drip tests at 90°C done under the unsaturated conditions expected at Yucca Mountain. Alteration of the

spent fuel was noted on a microscopic scale after 60 days of reaction and on a macroscopic scale after 748 days of reaction.

During the almost three years of testing, concurrent release of radionuclides was also noted. The magnitude of the radionuclide release in these tests was a function of several parameters including time. The following preliminary conclusions are drawn from release results for the first 581 days of reaction.

Congruent release of the radionuclides with $^{238}U$ was not noted during the first 581 days of reaction. An exception was the release of the transuranics, $^{239}Pu$, $^{237}Np$, and $^{241}Am$, from the ATM-106 fuel. The $^{238}U$ release fractions were much lower than those for $^{99}Tc$, $^{129}I$, $^{90}Sr$, and $^{137}Cs$. Since after 748 days of reaction there was macroscopic evidence for the formation of alteration products, the release results may indicate that the fuel matrix dissolved congruently under the conditions of our test, but, because of the low water inventory in the drip tests, many of the radionuclides were reprecipitated on the fuel or the Zircaloy fuel holder. Only those isotopes with very high solubilities in acidic solutions (the pHs in our tests) were found in the leachate collected in the test vessel.

The different release fractions observed for the different radioisotopes suggest that the four fission products (Cs, Sr, Tc, I) were affected differently by the conditions in these tests. The possible parameters included water chemistry, i.e. acidic pH. The cumulative and 581 day-interval $^{90}Sr$ release fractions were comparable to the $^{137}Cs$ release fractions for both fuels. For the ATM-103 fuel, the $^{99}Tc$ release fractions were two orders of magnitude larger than the $^{137}Cs$ release fractions. These large $^{99}Tc$ release fractions may be associated with rapid aqueous oxidation and dissolution of this fuel. The cumulative $^{129}I$ release fractions were two orders of magnitude larger than the $^{137}Cs$ release fractions for both fuels. Release in the earlier reaction intervals, which had the highest $^{129}I$ release fractions may be dominated by release from the gap and grain boundaries. Later release fractions may be dominated by release from the $UO_2$ matrix. The large fractional releases for $^{99}Tc$ may then reflect actual matrix dissolution under the conditions present in our tests. These results would suggest that uranium release fractions do not reflect matrix dissolution for low water-volume flow rates, typical of unsaturated testing conditions, nor the release fraction of highly soluble species. This observation may impact some of the assumptions made concerning the magnitude of the source term in performance assessment studies.

Most transport models assume that release of the individual radionuclides is congruent with that of the spent fuel matrix. From our results this assumption can be neither confirmed nor negated. Additional testing is required to determine if the variable releases at the 581 day-interval are representative of long term release behavior.

Colloidal species containing americium and plutonium have been found in the leachate of the drip tests, which simulate the unsaturated geological environment. These results suggest that significant quantities of colloids can form and may provide a mode of transport for the transuranics. Therefore, the incorporation of colloidal transport in performance assessment models is needed to ensure that the models have conservative transport limits.

Two fragments of reacted spent fuel were examined by scanning electron microscopy (SEM): ATM-103 and ATM-106. Based on crystal morphology, chemical composition as determined by energy-dispersive X-ray spectroscopy (EDS), and X-ray powder diffraction (XRD), the most abundant alteration product of spent fuel after 3.7 years of reaction is Na-boltwoodite, $(Na,K)(UO_2)(SiO_4)(H_3O)\cdot H_2O$. Additional minor phases have been detected by analytical electron microscopy (AEM) and XRD analyses, the most abundant of which is uranophane, $Ca(UO_2)(SiO_3)(OH)_2\cdot 5H_2O$ (~10 vol.%); however, Na-boltwoodite comprises greater than ~80 vol.% of the alteration products identified (a Cs-Mo-uranyl phase was found on the Zircaloy stand removed from the test vessel at 1.8 years).

Figures 2.1.3.5-2 shows a cross-section through a fragment of the ATM-103 fuel. This is the only fragment studied to date, and final conclusions must be based on a representative number of fragments. Nevertheless, the SEM image shows the fuel (brightest region) in which the grain boundaries are readily visible. Gaps of approximately 0.5 μm or less are visible between the fuel grains. No alteration phases between the grain boundaries have been detected, and Si is not evident from EDS analyses at the grain boundaries, indicating that dissolved Si is depleted in fluids penetrating the grain boundaries, probably due to the formation of uranyl silicates on the outer surface of the fuel.

Surrounding the fuel is an alteration layer consisting of predominantly Na-boltwoodite. The thickness of the layer varies but is approximately 20-40 μm. This Na-boltwoodite layer consists of two regions that differ in appearance: a dense layer, approximately 10 μm thick, closest to the fuel surface and a much less dense outer layer, 10–30 μm thick. No difference in composition is evident between the two layers using EDS. Near the outer edge of the denser (inner) layer is an interface (arrow, Fig. 2.1.3.5-2b) defined by a gap (dark band) that lies approximately 10 mm above the fuel surface and 2-3 mm below the outer edge of the dense layer. Just below this interface, crystals of Na-boltwoodite have formed more or less perpendicular to the fuel surface; whereas, above this interface, Na-boltwoodite forms the dense mat of crystals sub-parallel to the fuel surface. Above these flat lying crystals is the low-density outer layer. The inner region of the dense layer shows several curvilinear features that may be pre-existing grain boundaries. This leads us to believe that the inner, dense layer represents a region where the spent fuel has been replaced pseudomorphically (the iso-volumetric replacement of a pre-existing material that preserves the morphology of that material) by the Na-boltwoodite. The different densities of the two layers are manifested as different colors under optical examination: the inner layer is dark yellow, and the outer layer

is pale yellow to white. The inner layer is attached strongly to the adjacent fuel grains, whereas the outer layer is not.

Discussion

These preliminary data lead to the following discussion. The interface indicated in Fig. 2.1.3.5-2b (arrow) is interpreted as corresponding the position of surface of the original fuel fragment. Na-boltwoodite precipitated on the fuel surface, forming a mat of flat-lying crystals, and as the fuel dissolved, Na-boltwoodite replaced the fuel pseudomorphically. There is approximately a four-fold volume increase between cubic $UO_2$ and monoclinic Na-boltwoodite, so that (at most) 1/4 of the U in the replaced outer fuel layer is incorporated in the Na-boltwoodite within the replacement layer. The remaining 3/4 of the U was transported out of the replaced region, where much of it precipitated as Na-boltwoodite comprising the outer, less dense layer. However, Na-boltwoodite is not sufficiently dense to contain all the U that was lost from the reacted layer. Based on an estimate of the density of the Na-boltwoodite in Fig. 2.1.3.5-2a, the outer layer probably contains only about one half of the U lost from the reacted layer (i.e., ~38%). Some U is adsorbed on the vessel walls and is associated with the retainer, and there may be a buildup of alteration phases elsewhere in the test vessel.

There appears to have been extensive dissolution along grain boundaries, as evident from the friable nature of the fuel fragment when removed from the test vessel, and the wide gaps between grains (Fig. 2.1.3.5-2) (the expansion of the gaps between grains is enhanced by the oxidation of $UO_2$ to $UO_{2.25}$, but this cannot account fully for the observed widths of the gaps). However, dissolution along grain boundaries appears to be limited compared to the "through-grain" dissolution of the $UO_2$ grains, as indicated by the lack of embayment at grain-boundaries (Fig. 2.1.3.5-2). The replacement of the fuel has proceeded uniformly inward from the original outer surface (arrow in Fig. 2.1.3.5-2b) without regard to grain boundaries. Thus, the through-grain dissolution of the $UO_2$ fuel matrix may predominate over grain boundary-enhanced dissolution at this stage of reaction and has resulted in the pseudomorphic replacement of spent fuel by (predominantly) Na-boltwoodite. Note, however, that the volume of fuel reacted along grain boundaries within the fuel grains may be quite large compared to a uniform ~10 μm-thick replacement layer (see below).

The (simplified) reaction for the oxidative dissolution of the $UO_2$ fuel can be written as:

$$UO_2 + 2H^+ + 1/2O_2 \Rightarrow UO_2^{2+} + H_2O \qquad 2.1.3.5\text{-}1$$

The precipitation of Na-boltwoodite is:

$$UO_2^{2+} + H_4SiO_4 + Na^+ + H_2O \Rightarrow Na(UO_2)(SiO_4)(H_3O) + 3H^+ \qquad 2.1.3.5\text{-}2$$

Thus the *net* reaction for the replacement of the $UO_2$ fuel by Na-boltwoodite:

$$UO_2 + H_4SiO_4 + Na^+ + 1/2O_2 \Rightarrow Na(UO_2)(SiO_4)(H_3O) + H^+ \qquad 2.1.3.5\text{-}3$$

The last reaction (which is not an equilibrium expression) shows that, as Na- and Si-rich EJ-13 water is added to the system (i.e., to react with the $UO_2$ fuel), and/or $H^+$ is removed (due to flowing water and/or reaction with fuel via the first reaction), the replacement reaction proceeds to the right, provided that a sufficient supply of oxidants is available. In fact, an abundant supply of oxidants is likely available due to the effects of radiolysis and $O_2$ in the reaction vessel atmosphere.

The approximate volume of fuel that has been replaced can be calculated, based on our SEM observations. The estimated original geometric surface area is 2.1 $x10^{-4}$ $m^2/g$. The original mass of fuel is 8 g, giving an original total surface area of 0.00168 $m^2$. Assuming that the fragment of ATM-103 shown in Fig. 2 is representative of the reacted fuel surface, i.e., that the outer 10 μm of the entire fuel surface has been replaced by Na-boltwoodite, the estimated volume of fuel that has reacted is 1.68 x $10^{-8}$ $m^3$. The void volume is estimated to be ~50%. This corresponds to the release of 0.02 g of $UO_2$ ($\rho_{UO2}$ = 10.6 $g/cm^3$) [assuming a four-fold volume increase in going to boltwoodite and the 50% void fraction or a fractional release of approximately 0.24% of the total inventory of U in the fuel (Table 2.1.3.5-1). After 3.7 years this corresponds to an intrinsic rate of 70 $mg{\cdot}m^{-2}{\cdot}d^{-1}$, or a an *average* fractional release rate of 1.8 x $10^{-4}$ % per day *from the reacted layer* . This is only about twice the rate predicted by the best model in Section 3.4.2 at 90°C and groundwater carbonate concentrations. To this, one must add the additional mass of U released due to dissolution along grain boundaries. Based on Tc release, approximately 0.25 g of $UO_2$ has reacted, so that the mass of U corresponding to the replacement volume (0.02 g) represents ~8% of the total. That is, approximately 90% of the total U released from the fuel was derived from dissolution along the grain boundaries. Only ~1% of the U estimated to have reacted (based on Tc release) is found in solution, thus ~99% of the reacted U is contained in alteration products and on the vessel and retainer walls. At most, the alteration layer (both layers) observed by SEM contains approximately 50% of the U not accounted for in solution, meaning another ~50% is held up elsewhere.

## Summary

Reaction patterns for spent fuel differ from those of $UO_2$ in that sample alteration occurs along a uniform front that progressively penetrates into the spent fuel fragments, whereas $UO_2$ pellet dissolution occurs along the boundaries between the original press-sintered $UO_2$ grains. Dissolution rates for both the spent fuel and $UO_2$ samples were rapid in the present tests; however, most of the released uranium, and a significant portion of the fission products released from the spent fuel, were incorporated into alteration products that formed during sample reactions.

The data presented for spent fuel are preliminary and are surprising in that the predominant mode of corrosion is through grain dissolution accompanied by reaction of the grain boundary regions without subsequent conversion to alteration phases. Thus, the corrosion of spent fuel is more complicated than anticipated. The retention of fission products and actinides cannot be predicted at this time without further examination of additional grains and fragments of reacted fuel, an understanding of the grain boundary penetration and the increase of surface area, and the distribution of radionuclides between reacted phases and solution. While our studies suggest that the alteration phases will incorporate a large proportion of the radionuclides that have been released from dissolved spent fuel, and that such a process may act as a significant mechanism for retarding the migration of radionuclides from the waste package, synergistic effects between the waste form and parameters affecting its corrosion, with other components of the repository, must be taken into account before using the present data in predicting the fate of radionuclides in a repository.

## 2.1.3.5.5 REFERENCES


Bates, J.K., J. A. Fortner, P.A. Finn, D.J. Wronkiewicz, J.C. Hoh, J.W. Emery, E.C. Buck and S.F. Wolf (1995) "Yucca Mountain Project-Argonne National Laboratory, Annual Progress report, FY 1995," Argonne National Laboratory Report ANL-95/xx (August 1995). YMP Milestone 209, Accesion # MOL.19960620.0123

Grambow, B. (1989) "Spent Fuel Dissolution and Oxidation. An Evaluation of Literature Data," SKB Technical Report 89-13.

Grambow B., A. Loida, P. Dressler, H. Geckeis, J. Gago, I. Casas, J. de Pablo, J. Giménez and M. E. Torrero (1996) "Long-Term Safety of Radioactive Waste Disposal: Chemical Reaction of Fabricated and High Burnup Spent $UO_2$ Fuel with Saline Brines," Forschungscentrum Karlsruhe GmbH Report FZKA 5702.

Gray, W.J., and L. E. Thomas (1992) "Dissolution Rates of As-Received and Partially Oxidized Spent Fuel," High-level Radioactive Waste Management: Proceedings of the Third International Conference, pp. 1458-1464. American Nuclear Society, Inc., La Grange Park, Illinois.

Gray, W.J., L. E. Thomas and R. E. Einziger (1993) "Effects of Air Oxidation on the Dissolution Rate of LWR Spent Fuel," Sci. Basis for Nucl.Waste Management XVI, Vol. 294 [Eds. C.G. Interrante and R.T. Pabalan] pp. 47-54. Materials Research Society, Pittsburgh, Pennsylvania.

Gray, W.J., and Thomas, L.E. (1994) "Initial Results from Dissolution Testing of Various Air-Oxidized Spent Fuels," Sci. Basis for Nucl.Waste Management XVII, Vol. 333 [Eds. A. Barkatt and R.A. Van Konynenburg] pp. 391-398. Materials Research Society, Pittsburgh, Pennsylvania.

Gray, W.J. and C.N. Wilson (1995) "Spent Fuel Dissolution Studies FY1991 to 1994," Pacific Northwest National Laboratory Report PNL-10540 (December 1995).

Gray, W.J. (1996) "FY 1996 Letter Report on Spent Fuel Dissolution Studies," Pacific Northwest National Laboratory, Informal YMP Status Report (September 1996).

Steward, S.A. and W. J. Gray (1994) "Comparison of Uranium Dissolution Rates from Spent Fuel and Uranium Dioxide," Proc. 5th Annual Intl. High-Level Radio. Waste Mgmt. Conf., Las Vegas, Nevada, May 22-26, 1994, Vol. 4, pp. 2602-8, [Lawrence Livermore National Laboratory Report UCRL-JC-115355 (February 1994)].

Wilson, C.N. (1984) "Results from NNWSI Series 1 Spent Fuel Leach Tests," Report HEDL-TME 84-30, Hanford Engineering Development Laboratory, Richland, Washington. NNA.900216.0070.

Wilson, C.N. (1990a) "Results from NNWSI Series 3 Spent Fuel Dissolution Tests," Report PNL-7170 (June 1990), Pacific Northwest Laboratory, Richland, Washington.

Wilson, C.N. (1990b) "Results from NNWSI Series 2 Spent Fuel Dissolution Tests," Report PNL-7169 (September 1990), Pacific Northwest Laboratory, Richland, Washington.

Wilson, C.N. and C. J. Bruton (1990) "Studies on Spent Fuel Dissolution Behavior Under Yucca Mountain Repository Conditions," Ceramic Transactions, Vol. 9, pp. 423-442. Nuclear Waste Mgt. III (G. B. Mellinger, Ed.) Westerville, Ohio.

Wilson, C.N. and W. J. Gray (1990) "Effects of Water Composition on the Dissolution Rate of UO2 Under Oxidizing Conditions," High-level Radioactive Waste Management: Proceedings of the (First) International Topical Meeting, pp. 1431-1436. American Nuclear Society, Inc., La Grange Park, Illinois.

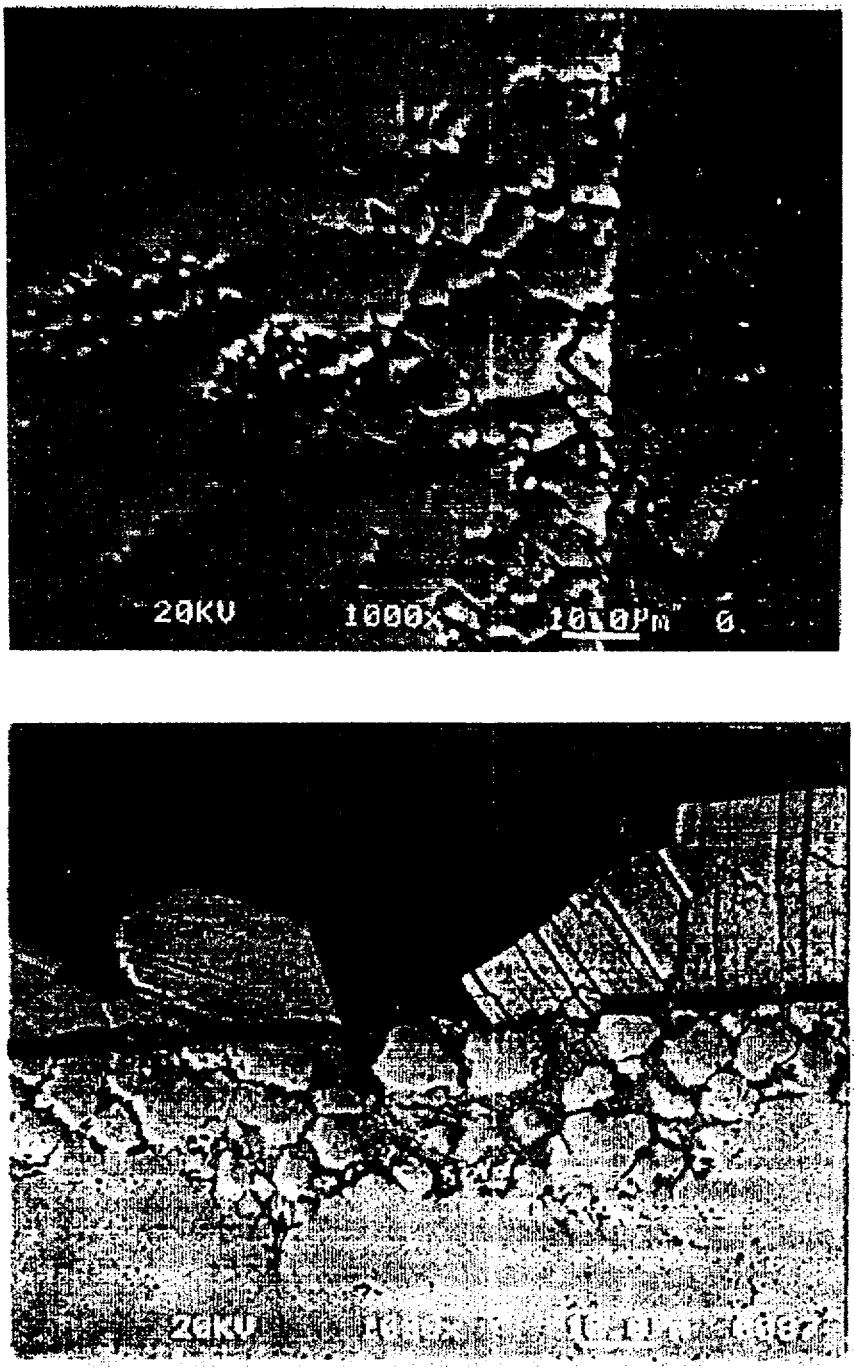


Figure 2.1.3.5-1. Scanning Electron Photomicrographs of Cross-Sectioned Corroded $UO_2$ Pellet Samples: (a) Open porosity resulting from penetrative intergrannular corrosion along pellet sides from the 3.5-year sample. Surface phase (gray color) is dehydrated schoepite. (b) Precipitation of compreignacide on top surface of the 8-year sample. Note the continuation of crystal delamination planes into the open porous region of the sample and the encapsulation of the residual $UO_{2+x}$ surface grains by the alteration phases.

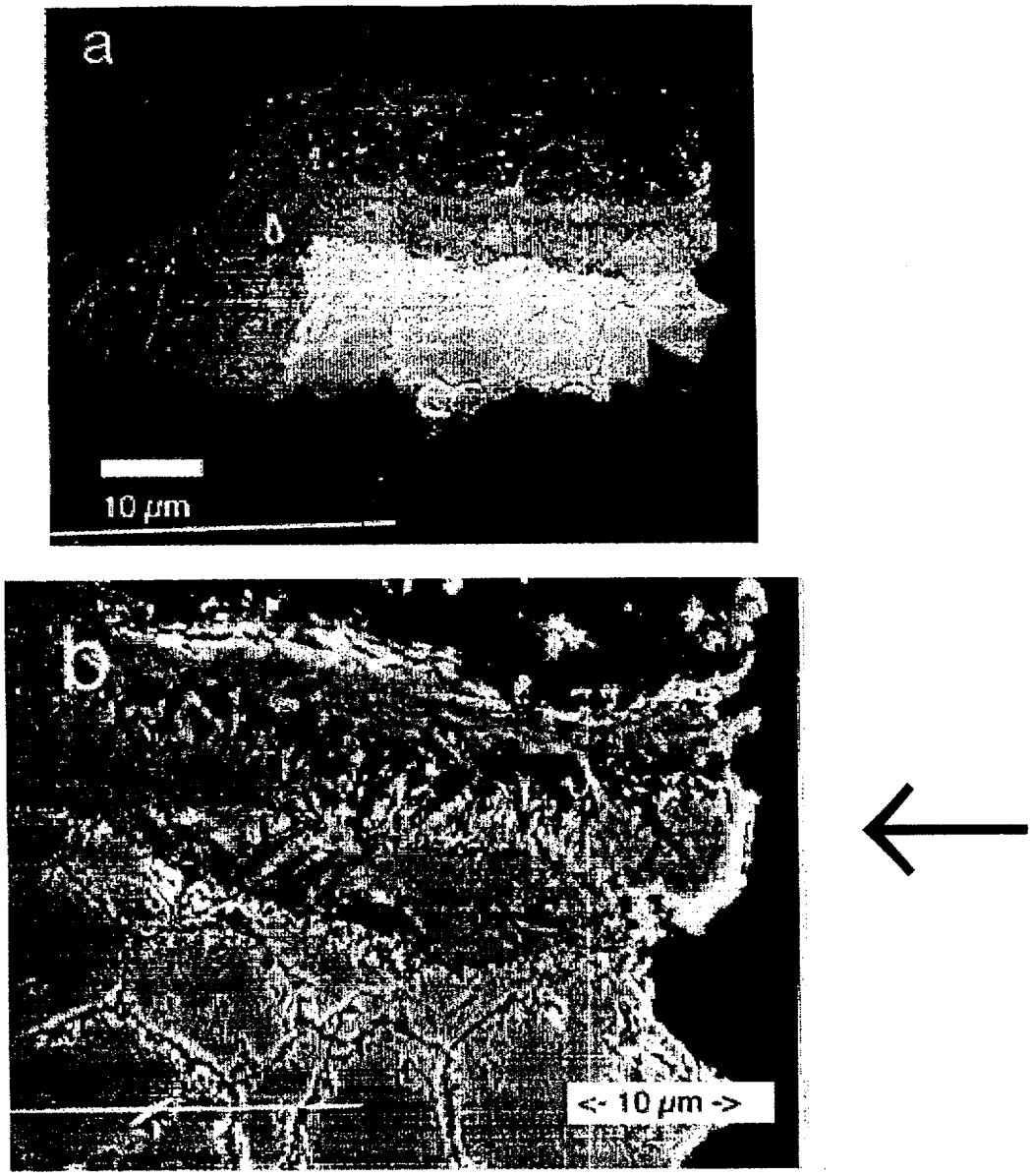


Figure 2.1.3.5-2. BSE Images of a Cross-Section through a Reacted Fuel Fragment of ATM-103 after 3.7 Years. Brightest contrast shows fuel grains (lower part of images) displaying expanded grain boundary gaps. The medium contrast is primarily Na-boltwoodite. Darkest contrast is epoxy. (b) is a magnified view showing the right side of (a). The arrow beside (b) is interpreted as corresponding to the position of the original fuel surface. The relatively dense layer below is the fuel replaced pseudomorphically by Na-boltwoodite; above is Na-boltwoodite precipitated at/and above the original surface of the reacting fuel. Note the lack of embayment of grain boundaries at the surface of the fuel in contact with the Na-boltwoodite. Relict grain boundaries in the replacement layer do not necessarily show a 1:1 correspondence to the fuel-grain boundaries due to the large volume change of the replacement reaction.

# STUDIES ON SPENT FUEL DISSOLUTION BEHAVIOR* UNDER YUCCA MOUNTAIN REPOSITORY CONDITIONS

C. N. Wilson
Pacific Northwest Laboratory

C. J. Bruton
Lawrence Livermore National Laboratory

## ABSTRACT

Nuclide concentrations measured in laboratory tests with PWR spent fuel specimens in Nevada Test Site J-13 well water are compared to equilibrium concentrations calculated using the EQ3/6 geochemical modeling code. Actinide concentrations in the laboratory tests reach steady-state values lower than those required to meet Nuclear Regulatory Commission (NRC) release limits. Differences between measured and calculated actinide concentrations are discussed in terms of the effects of temperature (25°C to 90°C), sample filtration, oxygen fugacity, secondary phase precipitation, and the thermodynamic data in use. The concentrations of fission product radionuclides in the laboratory tests tend to increase continuously with time, in contrast to the behavior of the actinides.

## 1.0 INTRODUCTION

The Yucca Mountain Project of the U. S. Department of Energy is studying the potential dissolution and radionuclide release behavior of spent fuel in a candidate repository site at Yucca Mountain, Nevada. The repository horizon under study lies in the unsaturated zone 200 to 400 meters above the water table. With the exception of C-14, which may migrate in a vapor phase,[1] and possibly I-129, the majority of long-lived radionuclides present in spent nuclear fuel will be transported from a failed waste package in the repository via dissolution or suspension in water in the absence of a major geological event such as volcanism.

*This material also is important in understanding Section 3.4.

[1]Published in Ceramic Transactions, V-9, pp. 423-442. Nuclear Waste Mgt. III, G. B. Mellinger, ed. Westerville, Ohio, 1990.

Spent fuel will not be contacted by liquid water infiltrating the rock until several hundred years after disposal when the repository has cooled to below the 95°C boiling temperature of water at the repository elevation. The potential dissolution behavior of spent fuel during the repository post-thermal period is being studied using geochemical models and laboratory tests with actual spent fuel specimens.* Selected initial results from these studies are discussed in the present paper.

## 2.0 LABORATORY TESTS

Three spent fuel dissolution test series have been conducted in laboratory hot cells using spent fuel specimens of various configurations. Results from the Series 2 and Series 3 tests with bare fuel particles are discussed in the present paper. The Series 2 tests used unsealed fused silica test vellels and were run for five cycles in air at ambient hot cell temperature (25°C). The Series 3 tests used sealed stainless steel vessels and were run for three cycles at 25°C and 85°C. Each test cycle was started in fresh Nevada Test Site J-13 well water and was about six months in duration. Periodic solution samples were taken during each test cycle and the sample volume was replenished with fresh J-13 water. Five bare fuel specimens tested in these two tests series are identified in Table 1 and the test configurations are shown in Figure 1. Additional information on the laboratory tests is provided in references 3 and 4.

### 2.1 Actinide Results

Actinide concentrations (U, Np, Pu, Am and Cm) measured in solution samples rapidly reached maximum levels during the first test cycle and then generally dropped to lower steady-state levels in later test cycles. The concentrations of uranium and the activities of Pu-239+240 and Am-241 measured in 0.4 mm filtered solution samples are plotted in Figure 2. The initial concentration peaks are attributed to dissolution of more readily soluble $UO_{2+x}$ oxidized phases present initially of the fuel particle surfaces, and to kinetic factors limiting the nucleation and growth of secondary phases that may ultimately control actinide concentrations at lower levels.

---

* This work was performed under the auspices of the U. S. Department of Energy (DOE) by Lawrence Livermore National Laboratory under Contract No. W-7405-Eng-48, and by Pacific Northwest Laboratory operated for the DOE by Battelle Memorial Institute under Contract No. DE-AC06-76RLO-1830

**Table 1. Bare Fuel Test Identification**

| identification | Description | Starting Fuel Wt. (g) |
|---|---|---|
| HBR-2-25 | Series 2, H.B. Robinson Fuel, 25°C | 83.10 |
| TP-2-25 | Series 2, Turkey Point Fuel, 25°C | 27.21 |
| HBR-3-25 | Series 3, H.B. Robinson Fuel, 25°C | 80.70 |
| HBR-3-85 | Series 3, H.B. Robinson Fuel, 85°C | 85.55 |
| TP-3-85 | Series 3, Turkey Point Fuel, 85°C | 86.17 |

Uranium (U) concentrations at 25°C were lower in the Series 3 tests than in the Series 2 tests, and with the exception of the Cycle 1 data, U concentrations in the 85°C Series 3 tests were lower than those in the 25°C tests. The very low U concentrations measured during Cycle 1 of the HBR-3-85 test were attributed to a vessel corrosion anomaly. In the later cycles of the Series 2 tests, U concentrations tended to stabilize at steady-state levels of about 1 to 2 μg/ml. In Cycles 2 and 3 of the Series 3 tests, U concentrations stabilized at about 0.3 μg/ml at 25°C and about 0.15 μg/ml at 85°C. Precipitated crystals of the calcium-uranium-silicates, uranophane (Figure 3) and haiweeite, and possibly the uranium-silicate soddyite, were found on filters used to filter cycle termination rinse solutions from both 85°C tests. Phase identifications were based on examinations by X-ray diffraction and microanalysis in the SEM.[4] Secondary phases controlling actinide concentrations other than U were not found.

The 0.4 μm filtered Pu-239+240 solution activities measured in Cycles 2 through 5 of the TP-2-25 test generally ranged from about 100 to 200 pCi/ml (Figure 2). Activities as low as about 20 pCi/ml were measured in the HBR-2-25 test. During Cycles 2 and 3 of the HBR-3-25 test, activities varied from about 60 to 1 00 pCi/ml. A value of 100 pCi/ml, which corresponds to a Pu concentration of about $4.4 \times 10^{-9}$ M (M = molarity), would appear to be a reasonable estimate of steady-state Pu-239+240 activities in 0.4 μm filtered solutions in the 25°C. Significantly lower activities on the order of 1 pCi/ml were measured in the 85°C tests. The lower activities at 85°C may result from enhanced nucleation and growth of secondary phases at the higher temperature that limit pU concentration.

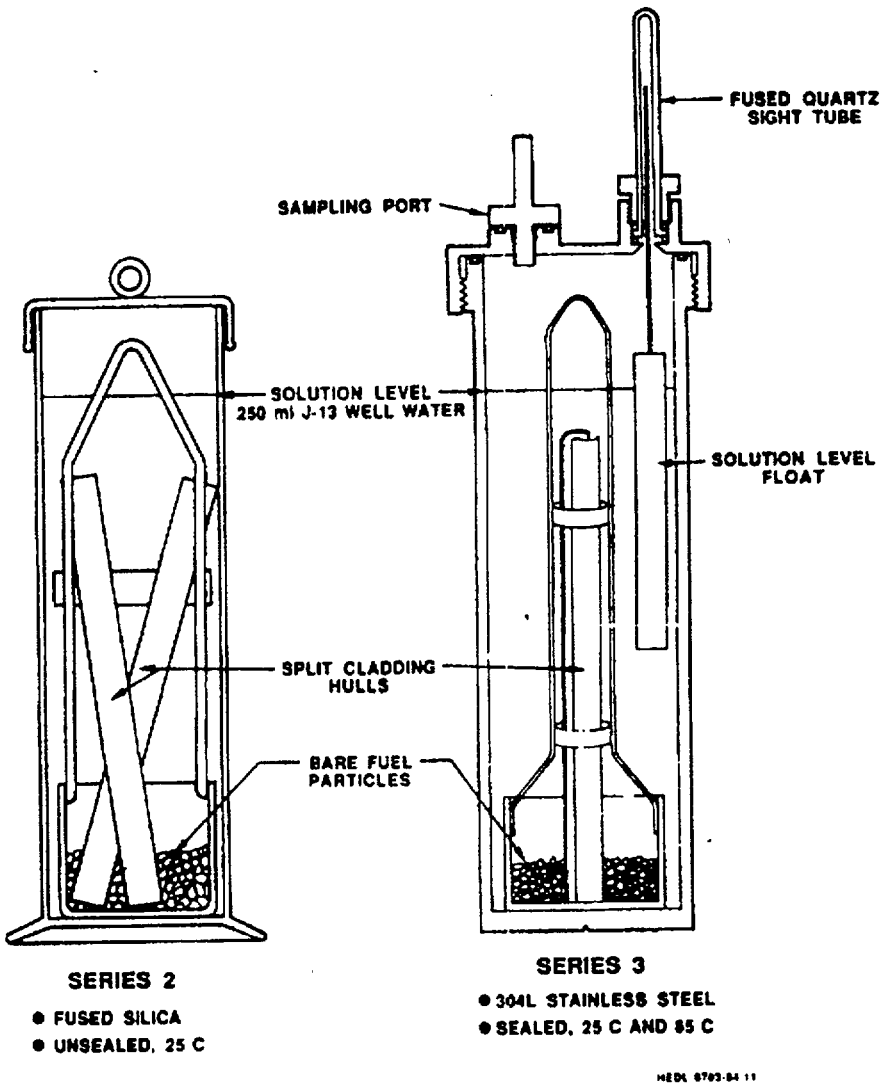


**Figure 1.** Test Configurations for the Series 2 and Series 3 Bare Fuel Dissolution Tests.

Selected solution samples were centrifuged through membrane filters that provide an estimated filtration size of approximately 2 nm.* Filtering to 2 nm caused Pu-239+240 activities to decrease by about 20 to 40%. No significant differences between 0.4 μm filtered sample data are considered the most significant relative to radionuclide release because larger particles probably would not be transported by water, whereas colloidal particles greater than 2 nm may remain in stable suspension and be transported by water movement.

**Table 2. J-13 Well Water Analysis[2]**

| Component | Concentration (μg/ml) | Component | Concentration (μg/ml) |
|---|---|---|---|
| Li | 0.042 | Si | 27.0 |
| Na | 43.9 | F | 2.2 |
| K | 5.11 | Cl | 6.9 |
| Ca | 12.5 | $NO_3$ | 9.6 |
| Mg | 1.92 | $SO_4$ | 18.7 |
| Sr | 0.035 | $HCO_3$ | 125.3 |
| Al | 0.012 | | |
| Fe | 0.006 | pH | 7.6 |

Steady-state Am-241 activities on the order of 100 pCi/ml, corresponding to Am concentrations of about $1.5 \times 10^{-10}$ M, were measured in 0.4 μm filtered samples during cycles 2 and 3 of the TP-2-25 and HBR-3-25 tests. The 100 pCi/ml value would appear to be a conservative estimate for Am-241 activity at steady-state and 25°C considering that activities on the order of 10 pCi/ml were measured during Cycles 2, 4 and 5 of the HBR-2-25 test. Much lower 0.4 μm filtered Am-241 activities of about 0.3 pCi/ml were measured during Cycles 2 and 3 of the two 85°C tests. The effects of both 0.4 μm and 2 nm filtration were in general greater for Am-241 than for Pu-239+240. Association of Am with an apparent suspended phase is suggested by unfiltered data from the 85°C tests plotted as dashed lines in Figure 2, and by a relatively large fraction of 0.4 μm filtered Am-241 activity removed by 2 nm filtration (not shown). Cm-244 activity measured in most samples was similar to that measured for Am-241 in each of the tests. However, Cm-244 alpha decays with an 18-year half-life to Pu-240 and will not be present during the repository post-thermal period.

Measured Np-237 activities in most samples were generally not much greater than the detection limit of 0.1 pCi/ml and were below detection limits in several samples. Measured Np-237 activities showed very little dependence on temperature, vessel type or sample filtration. Following initially higher values at the beginning of Cycle 1, Np-237 activities generally ranged from 0.1 to 0.5 pCi/ml.

---

*Amicon Corporation Model CF-25 centrifuge membrane cone filter

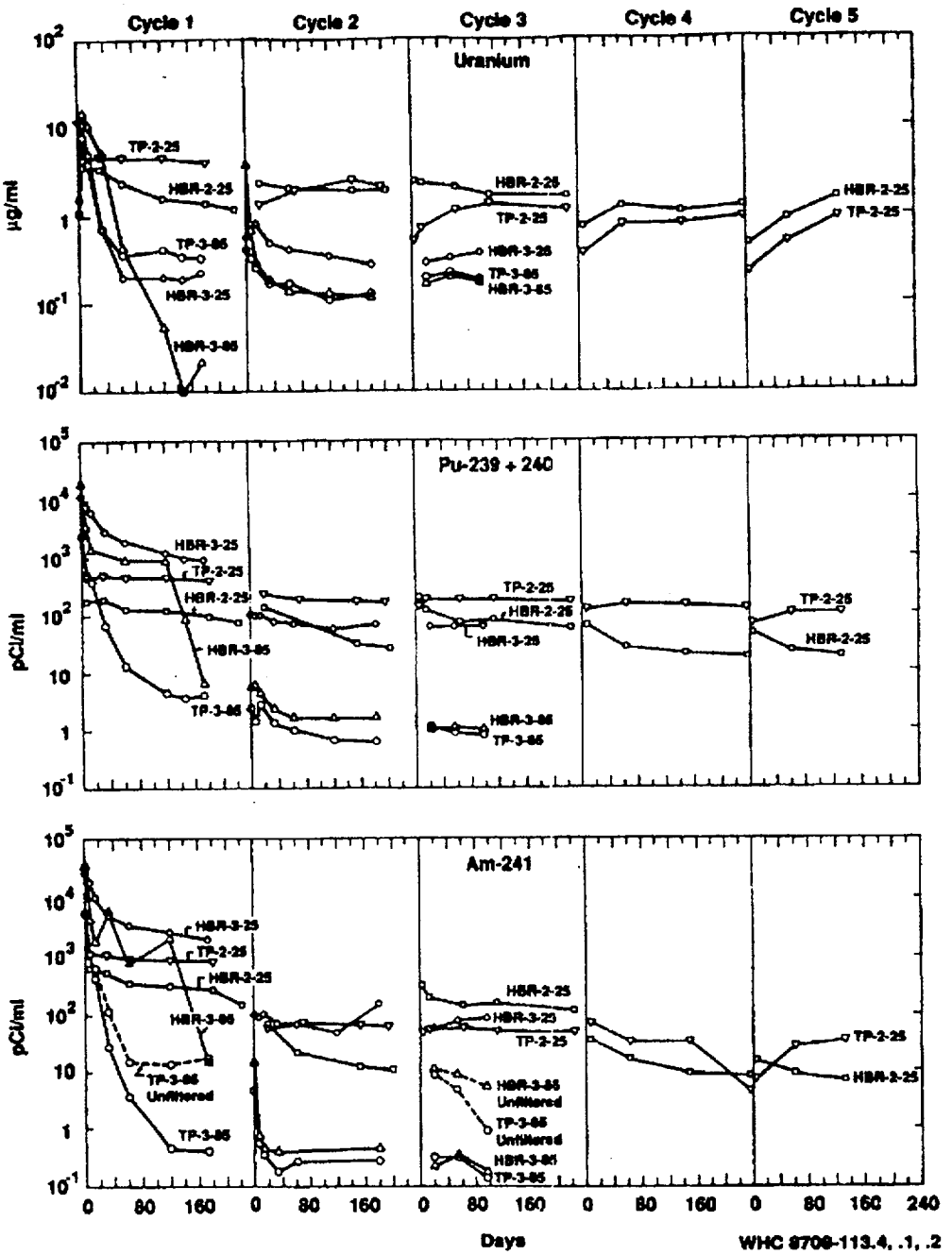


**Figure 2.** Uranium Concentrations (top), Pu-239+240 Activities (center), and Am-241 Activities (bottom); Measured in 0.4 µm Filtered Solution Samples.

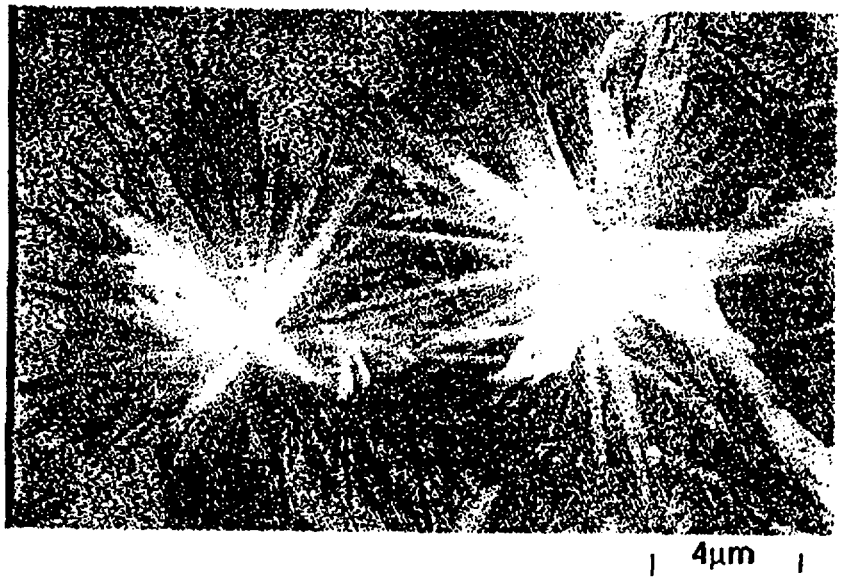


**Figure 3.** Acicular crystals of Uranophane formed on spent fuel grains in the 85°Series 3 tests.

## 2.2 Fission Product Results

Specimen inventory fractions of the fission product radionuclides Cs-137, Sr-90, Tc-99, and I-129 measured in solution are plotted in Figure 4 for the HBR-2-25 and HBR-3-85 tests. Each data point represents the fraction of the ORIGEN-2 calculated specimen inventory in solution on the sample data plus the inventory fraction calculated to have been removed in previous samples from the test cycle. During Cycle 1 of the HBR-3-85 test, Tc-99 fell to below detectable levels as a result of the corrosion anomaly that occurred in this test. Cycle 1 Cs-137 gap inventory release was about 0.7% from the HBR fuel and is therefore off-scale in Figure 4. Sr-90 was not measured during Cycle 1 of the Series 2 tests, and appeared to be limited by association with an unknown precipitated phase in the 85°C tests.

The inventory fractions of Cs-137, Sr-90, Tc-99 and I-129 in solution increased continuously with time, with the exception of the anomalous precipitation of Tc-99 in Cycle 1 of the HBR-3-85 test and the limit on Sr-90 activity in solution at 85°C. The continuous release rates of the fission products in units of inventory fraction per year are given in Figure 4 for the final cycle of the two tests. Because the actual quantity of fuel matrix dissolution and precipitation of actinides was not measured, it is not known to what degree the continuous fission product release resulted form preferential leaching of grain boundaries where fission products were thought to concentrate during irradiation. Whether as a result of increased matrix dissolution or increased grain boundary leaching, the soluble fission product release rate is greater in the later test cycles at the higher temperature.

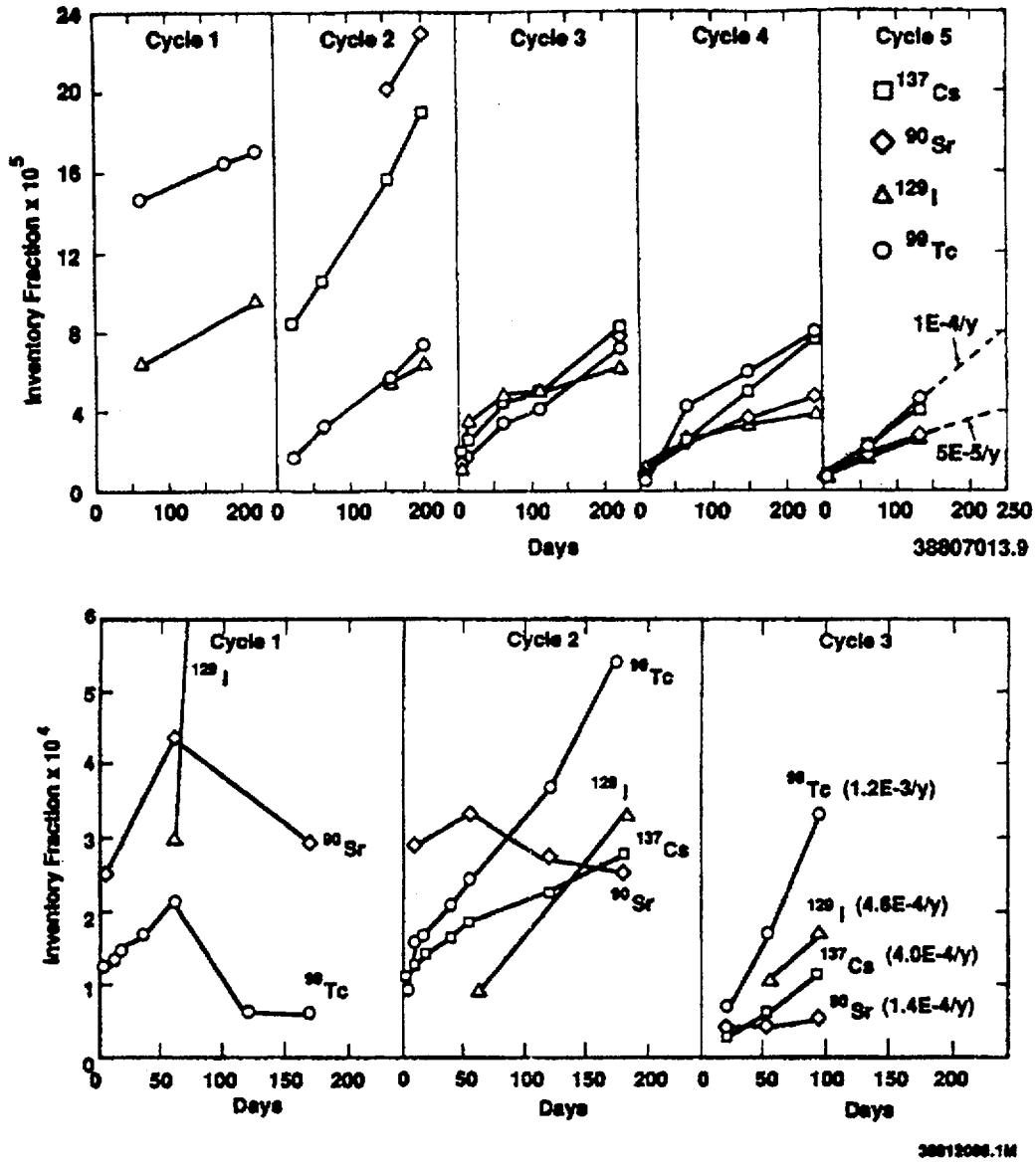


**Figure 4.** Inventory Fractions of Cs-137, Sr-90, Tc-99 and I-129 Measured in Solution in the HBR-2-25 Test (top) and in the HBR-3-85 Test (bottom). Approximate annual fractional release rates are listed for each nuclide during the last cycle plotted.

## 3.0 GEOCHEMICAL MODELING

### 3.1 Actinide Concentrations in Solution

Spent fuel dissolution in J-13 well water was simulated using the geochemical modeling code EQ3/6[5] to determine whether steady-state actinide concentrations measured in the tests could be related to the precipitation of actinide-bearing solids. Version 3245 of the EQ3/6 code and version 327OR13 of the supporting thermodynamic database were used to simulate spent fuel dissolution at 25°C and 90°C assuming atmospheric $CO_2$ gas fugacity and two different $0_2$ gas fugacities of $10^{-0.7}$ (atmospheric) and $10^{-12}$ bars (see later discussion). The simulation process is described in more detail elsewhere.[6] The computer simulations yield: 1) the sequence of solids that precipitate and sequester elements released during spent fuel dissolution, and 2) the corresponding elemental concentrations in solution. Approximate steady-state actinide concentrations measured at 25°C and 85°C in the Series 3 laboratory tests were compared in Table 3 to concentrations of actinides in equilibrium with the listed solids as calculated in the EQ3/6 simulations. Comparisons of simulation results with experimental results are being used to determine the adequacy of the thermodynamic database and to identify additional aqueous species and minerals for which data are needed.

**Table 3. Comparison of Measured and Predicted Actinide Concentrations (log M)**
(New runs have not been completed) May 22, 1993 RBS)

| | | | EQ3/6[b] | | | | |
|---|---|---|---|---|---|---|---|
| | Measured[a] | | 25°C | | 90°C | | |
| Actinide | -25°C | 85°C | -0.7 | -12.0 | -0.7 | -12.0 | Phase |
| U | -5.9 | -6.2 | -7.2/-7.0* | -7.1/6.9 | -8,8.-7.6 | -8.5/-7/5 | H |
| | | | -7.0/-6.9 | -6.9/-6/8 | -7/6 | -7.5 | H + S |
| | | | -6.9/-4.3 | -6.8/-4.2 | -7.6/-6.0 | -7.5/-5.9 | S |
| | | | -4.3 | -4.2 | -6.0 | -5.9 | S + Sch |
| | | | -4.2 | -4.1 | -6.0/-5.8 | -5.8/-5.6 | Sch |
| Np | -8.9 | -9.1 | -6.2 | -9.0 | -5.2 | -8.0 | $NpO_2$ |
| Pu | -8.4 | -10.4 | -12.4 | -13.8 | -11.9 | -14.6 | $PuO_2$ |
| | | | -4.3 | -5.7 | -4.2 | -6.9 | $Pu(OH)_4$ |
| Am | -9.8 | -12.3 | -8.3 | -8.3 | – | – | $Am(OH)CO_3$ |
| | | | – | – | -8.4 | -8.4 | $Am(OH)_3$ |
| Cm | -11.3 | -14.3 | Cm not in thermodynamic data base | | | | |

(a) Series 3 tests, 0.4 μm filtered.
(b) At oxygen fugacities log $f_{02}$ = -0.7 (atmospheric) and log $f_{02}$ = -12.0 with solubility control by precipitated secondary phases as listed. H = haiweeite; S = soddyite; Sch = schospite. All phases are in crystalline state except $Pu(OH)_4$ which is amorphous.
*-7.2/-7.0- refers to a range in concentration from -7.2 to -7.0.

Uranium (U) concentrations in the simulations vary as a function of the secondary U-bearing precipitates. The following sequence of mineral assemblages are predicted to precipitate and sequester U as increasing amounts of spent fuel dissolve: haiweeite, haiweeite plus soddyite, soddyite, soddyite plus schoepite, and schoepite. The relative compositions of these phases and of U-bearing phases that were observed in residues from the 85°C laboratory tests are shown in Figure 5. Unique, and steadily increasing, concentrations of U in solution are related to each mineral assemblage. The concentration of U varies not only as the precipitates vary, but also during the precipitation of a single mineral, such as soddyite, because of changes in the pH and overall chemical characteristics of the fluid. As previously discussed, uranophane, haiweeite, and possibly soddyite were found in the 85°C Series 3 tests. Unfortunately, reliable thermodynamic data for uranophane were not available, which complicates comparison of the laboratory test results to the calculated solubility limits. Haiweeite, aCa-U-silicate like uranophane, is predicated to precipitate at U concentrations that are lower than the measured steady-state values. In the absence of data for uranophane, the experimental concentrations of U would appear to be consistent with the precipitation of soddyite at both 25°C and 90°C in the simulations.

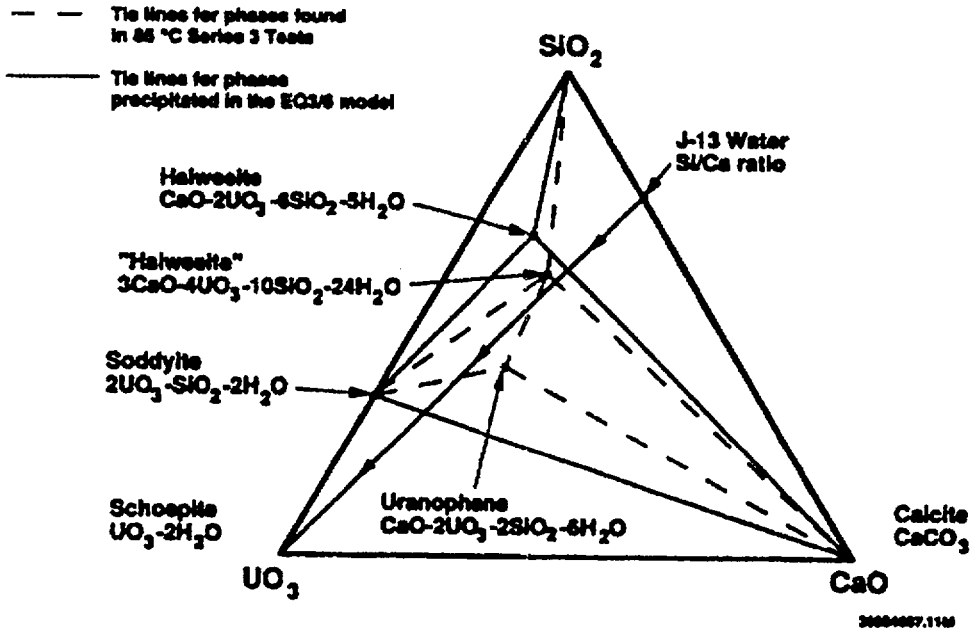


**Figure 5. Relative Compositions (mole %) of U-bearing Phases Indicated as Controlling U Concentration in the EQ3/6 Simulation and for which Indications were Observed in the 85°C Series 3 Tests.**

Neptunium concentration is controlled by equilibrium with $NpO_2$ in the simulations. However, the predicted concentration of Np is highly dependent on solution Eh and pH .[7] The $O_2$ fugacity in the simulations was reduced from $10^{-0.7}$ bars to $10^{-12}$ bars in order to produce good agreement between the measured and predicted concentrations of Np at 25°C. An $O_2$ fugacity of $10^{-12}$ bars may correspond to conditions at the fuel surface in an otherwise oxygenated system (i.e., contains an air cap) that is poorly buffered. Eh was not measured during the laboratory tests, and redox equilibrium may not have been established among the various species and phases within the sealed stainless steel vessels. An oxygen fugacity of $10^{-12}$ bars overestimates Np concentration at 90°C, however, because the experimental data do not reflect predicted increases in Np concentration with temperature. The thermodynamic data for Np and other actinides must, consequently, be critically evaluated at elevated temperature.

Significant differences exist between measured and predicted Pu and Am concentrations in Table 3. Measured Am concentrations may have been lower than those predicted because of Am removal from solution by phases such as lanthanide precipitates that were not accounted for in the E03/6 simulations. Another possible mechanism controlling Am concentration not accounted for in the simulation may have been sorption. Although $Am(OH)CO_3$ is predicted to control Am concentration at 25°C and Am $(OH)_3$ precipitates at 90°C, the Am concentration in equilibrium with both phases is about the same.

Predicted Pu concentrations in equilibrium with crystalline $PuO_2$ at both temperatures and oxygen fugacities are much lower than those measured. Pu concentrations measured at 25°C are similar to those reported by Rai and Ryan,[8] who measured the solubility of $PuO_2$ and hydrous $PuO_2 \lozenge xH_20$ in water for periods of up to 1300 days at 25°C. At a pH of 8, which was the extrapolated lower limit of their data and the approximate pH in the Series 2 and 3 tests, they reported that Pu concentrations ranged from about $10^{-7.4}$ M, where amorphous $PuO_2 \lozenge xH_20$ was thought to control concentration, down to about $10^{-9}$ M where aging of the amorphous material produced a more (but incompletely) crystalline $PuO_2$ that was thought to control concentration. Concentrations of Pu in equilibrium with amorphous $Pu(OH)_4$ calculated in recognition of the fact that an amorphous or less crystalline phase is more likely to precipitate than crystalline $PuO_2$, are listed in Table 3. Measured Pu concentrations would be expected to fall between the equilibrium concentrations for $PuO_2$ and $Pu(OH)_4$, becoming closer to $PuO_2$ with aging. Equilibrium with amorphous $Pu(OH_4)$ and crystalline $PuO_2$ at $0_2$ fugacities of $10^{-0.7}$ and $10^{-12}$ bars yields predicted Pu concentrations that bracket measured results at both 25°C and 85°C.

## 3.2 Sources of Discrepancy Between Measured and Predicted Results

Discrepancies between measured and predicted concentrations are to be expected considering database limitations and uncertainty in the interpretation of measured apparent steady-state actinide concentrations. Care must be taken in interpreting the 90°C simulation results because insufficient data exist to accurately calculate the temperature-dependence of the thermodynamic properties of many radionuclide-bearing solids and solution species. The 3270 thermodynamic data basis constantly updated through inclusion of new and revised thermodynamic data and the selection of a consistent set of aqueous complexes for reach chemical element. Puigdomenech and Bruno[9] have constructed a thermodynamic database for U minerals and aqueous species that they showed to be in reasonable agreement with available experimental solubility data in systems in which U is complexed by OH- and $CO_3$. The 3270 database contains many of the same aqueous species and minerals, but Puigdomenech and Bruno have included recent data for aqueous uranyl hydroxides from Lemire[10] which are not yet in the EQ3/6 database. Future plans include a critical evaluation of simulations of spent fuel dissolution made using the Puigdomenech and Bruno U database, and comparison with simulations made using the latest version of the EQ3/6 database. Inclusion of standard Nuclear Energy Agency (NEA) data for U minerals and species will also help to standardize future databases.

Until the U database is better established, calculated U concentrations must be recognized as preliminary and speculative. Simulation results can be used as a vehicle for identifying geochemical trends and studying the interactions between solid precipitation and elemental concentrations in solution. Seemingly small changes in the thermodynamic database can have potentially large impacts on predictions. For example, U concentrations calculated to be in equilibrium with schoepite using version 3270 of the E03/6 database are radically lower than those predicted in 1987[6] using an older database. The species $(U_2)_3(OH)_7^-$ and $(UO_2)_2(OH)_3CO_3^-$ were omitted from version 3270 of the EQ3/6 database because their validity was questioned. $UO_2(CO_3)_2^{-2}$ and $UO_2(CO_3)_3^{-4}$ were left as the only dominant U species in solution throughout the EQ3/6 simulations. U concentrations accordingly remain lower during U mineral precipitation. Future work must address the sensitivity of the results to variations in thermodynamic data and the choice of a self-consistent set of aqueous species for elements of interest.

Comparisons between experimental results and predictions in Table 3 are predicated on the assumption that the listed solid phases precipitate from solution and control the solution composition. Except for some U-bearing minerals, no minerals containing radionuclides have been identified in the laboratory tests. Detection and characterization of actinide-bearing secondary phases may be difficult because of the extremely small masses of these actinides involved. Precipitates limiting actinide concentrations in the laboratory tests may also be

amorphous, colloidal, or in some other less-than-perfect crystalline state. For instance, Rai and Ryan" observed that early Pu precipitates tend to be hydrated oxides which undergo aging to more crystalline solids. The concentrations of the affected actinides would, therefore, gradually decrease as aging progresses.

The chemistry of trivalent Am and Cm can be expected to be almost identical to that of the light lanthanide fission product elements which are present in much greater concentrations in spent fuel than are Am and Cm. Am and Cm may, therefore, be present in dilute solid solution with secondary phases formed by the lanthanides, which would result in lower measured solution concentrations than predicted for Am based on equilibration with $Am(OH)CO_3$ or $Am(OH)_3$. Pu and Np, and possibly Am and Cm, may also have been incorporated at low concentrations in solid solution with the U-bearing precipitates or other secondary phases. Efforts are planned to separate crystals of uranophane from test residues and to perform radiochemical analyses of these crystals to check for incorporation of other radionuclides. Sorption of actinides on colloids or other surfaces such as the fuel or test hardware may also control solution concentrations, but the impact or sorption was not considered in the simulations. Other factors, such as local variations in redox potential, may also contribute to differences between measured and predicted solubilities.

As it is not currently reasonable to expect a geochemical model to predict accurately the effects of all potential concentration-controlling processes over thousands of years, we hope to use modeling predictions to establish upper limits, or conservative estimates, of radionuclide concentrations over time. Lower limits to radionuclide concentrations imposed by solid precipitation are also of interest, however, as a baseline for further calculations, and because radionuclide concentrations may be expected to approach the lower limits over extended time periods. Accordingly, we assume in this paper that the actinide concentrations are controlled by the most stable and insoluble precipitates for which data are available. The consequences of precipitation of progressively less stable precipitates will be explored in future calculations, and upper limits of radionuclide concentrations controlled by solid precipitation will be estimated. In the case of Pu, for example, we have begun to explore the upper limits to Pu concentration as controlled by the precipitation of amorphous $Pu(OH)_4$. Comparison of modeling results with experimental results helps to identify phenomena which may revise our estimates of concentration limits. Processes such as sorption and aging of solids to forms of increasing crystallinity tend to lower element concentrations in solution, and increase the conservative nature of our estimates. However, consideration of colloid formation and colloid migration with the fluid phase may lead to an increase in our estimates of mobile concentrations over those made considering precipitation phenomena alone.

## 4.0 RADIONUCLIDE RELEASES

Annual actinide releases per failed waste package were calculated assuming that water flowing at a rate of 20 1/yr per waste package transports the actinides at the approximate concentrations measured at steady-state in Cycles 2 and 3 of the HBR-3-25 test. Each waste package was assumed to contain 3140 kg of fuel with an average burnup of approximately 33,000 MWd/MTM. The logarithms of the waste package 1000-year inventory fractions transported annually for each actinide under such conditions is given in Table 4. These releases are at least three orders of magnitude lower than the Nuclear Regulatory Commission (NRC) requirement in 10 CRF 60.113[11] that annual radionuclide releases during the post-containment period shall not exceed one part in 100,000 of the 1000-year inventories. The calculated annual release results would appear to be particularly encouraging for Pu and Am because isotopes of these two actinide elements account for about 98% of the total activity present in spent fuel at 1000 years. These values may be conservative in that they are based on the higher steady-state Pu and Am concentrations measured at 25°C and assume a conservative (high) estimate of the water flux through the repository. The calculated releases do, however, assume maintenance of steady values for actinide concentrations over time, whereas the geochemical simulations suggest that actinide concentrations, and U concentrations in particular, may vary with time. Confidence in such release predictions will be greatly increased when the chemical mechanisms of solubility control are identified and successfully modeled.

Table 4. Annual Actinide Releases as a Fraction of the 1000-Year Inventories Based on HBR-3-25 Test Date

| Actinide | Concentration Log(M) | Log (Release)* |
|---|---|---|
| U | -5.9 | -8.6 |
| Np | -8.9 | -8.8 |
| Pu | -8.4 | -9.0 |
| Am | -9.8 | -9.1 |

*Assumes water flow rate of 20 1/yr per waste package transporting actinides at the indicated concentrations. Each waste package is assumed to contain 3140 kg of 33,000 MWd/MTM burnup PWR fuel.

Measured activities of the more soluble fission product radionuclides Cs-137, Sr-90, Tc-99 and I-129 continuously increase in solution at rates generally corresponding to annual release rates in the range of $10^{-4}$ to $10^{-3}$ of specimen inventory per year (Figure 4). These release rates imply a problem in meeting the NRC$10^{-5}$ annual fractional release limit for the more soluble radionuclides if the waste form alone is expecting to carry the burden of compliance in the unanticipated case of large quantities of water contacting the waste. However, there are two factors that make these release rates uncertain. First, the degree to which these radionuclides are preferentially released from grain boundaries where they may be concentrated during irradiation has not yet been determined. Preferential release could be expected to provide a lesser contribution over time as exposed grain boundary inventories are depleted and release rates approach the congruent fuel matrix dissolution rate. A second factor is the extent to which the fuel may be degraded over time by exposure to the repository environment. Degradation of the fuel as a result of oxidation to higher oxygen stoichiometries such as $U_3O_8$, or as a result of preferential grain boundary dissolution, may cause increases in surface area and increased rates of nuclide dissolution from grain boundaries and from the fuel matrix over time.

Flow-through tests in which uranium minerals do not precipitate are being developed to measure the degree to which soluble nuclides are preferentially released during the initial phases of fuel dissolution. Dissolution tests using spent fuel specimens that have been degraded by slow, low-temperature oxidation are also planned. Results from these tests should provide a better understanding of potential long-term releases of the soluble and volatile radionuclides. Additional characterization of potential release of C-14 is important because it is soluble as bicarbonate and could also be released in the vapor phase as $CO_2$.

## 5.0 CONCLUSIONS

Laboratory testing and geochemical simulation of the dissolution of spent fuel under conditions selected for relevance to the proposed Yucca Mountain repository have resulted in the following conclusions.

1. Radionuclides of interest in spent fuel appear to fall into three categories of potential release mechanisms: 1) radionuclides whose release appears to be controlled by concentration-limiting mechanisms, 2) more highly soluble radionuclides, and 3) radionuclides that are released in the vapor phase (principally C-14).

2. The principal radionuclides whose releases appear to be controlled by concentration-limiting mechanisms are the actinides U, Np, Pu, Am and Cm.

Steady-state concentrations measured for these actinide elements are at least three orders of magnitude lower than those required to meet NRC release limits based on conservative estimates of water fluxes through the repository. This result is of particular significance because isotopes of Pu and Am account for about 98% of the activity in spent fuel at 1000 years. However, results from geochemical modeling suggest that steady-state concentrations may vary significantly with time because of changes in solution composition and the identity of precipitating phases.

3. Good agreement between measured and predicted concentrations was obtained for Np based on equilibration with $NpO_2$ at 25°C when the oxygen fugacity in the simulation was set at $10^{-12}$ bars. A broad range of solubilities that bracketed the measured values were predicted for Pu depending upon the assumed oxygen fugacity and solubility-controlling phase. Measured Am concentrations were less than predicted based on data for equilibration with $Am(OH)CO_3$ and $Am(OH)_3$.

4. Dissolution rates for soluble radionuclides (Cs-137, Sr-90, Tc-99 and I-129) exceeding $10^{-5}$ of specimen inventory per year were measured during the laboratory tests. The implications of these data relative to long-term release of soluble radionuclides from a failed waste package are uncertain. The degree to which these radionuclides were preferentially released from grain boundaries where they may have concentrated during irradiation was not determined. Preferential release could be expected to provide a lesser contribution overtime as exposed grain boundary inventories are depleted. However, physical degradation of the fuel over time from exposure to the oxidizing repository environment may result in accelerated release of soluble nuclides.

5. Additional work is required to identify solid phases that control actinide concentrations, and to acquire reliable thermodynamic data on these phases for use in geochemical modeling. In this regard, identification of any stable suspended phases that can be transported by water movement is also important. In addition, we must better understand the potential release of soluble and volatile radionuclides, which may initially depend on preferential release from gap and grain boundary inventories, but may ultimately depend on the rate of fuel degradation by oxidation or other processes in the postcontainment repository environment.

REFERENCES


1. R. A. Van Konynenburg, C. F. Smith, H. W. Culham and C. H. Otto Jr., "Behavior of Carbon-14 in Waste Packages for Spent Fuel in a Repository in Tuff," Scientific Basis for Nuclear Waste Management VIII, C. M. Jantzen, J. A. Stone and R. C. Ewing, eds., Materials Research Soc., Pittsburgh, PA, 44:405-412 (1985).

2. J. M. Delany, Reaction of Topopah Spring Tuff with J-13 Water: A Geochemical Modeling Approach Using the EQ3/6 Reaction Path Code, Lawrence Livermore National Laboratory, UCRL-53631 (1985).

3. C. N. Wilson, Results from Cycles 1 and 2 of NNWSI Series 2 Spent Fuel Dissolution Tests, Hanford Engineering Development Laboratory, HEDL-TME 85-22 (1987).

4. C. N. Wilson, "Summary Results from the Series 2 and Series 3 NNWSI Bare Fuel Dissolution Tests," Scientific Basis for Nuclear Waste Management IX, M. J. Apted and R. E. Westerman, eds. Materials Research Soc., Pittsburgh, PA, 112:473-483 (1987).

5. T. J. Wolery, Calculation of Chemical Equilibrium Between Aqueous Solution and Minerals: The EQ3/6 Software Package, Lawrence Livermore National Laboratory, UCRL-52658 (1979).

6. C. J. Bruton and H. F. Shaw, "Geochemical Simulation of Reaction Between Spent Fuel Waste Form and J-13 Water at 25°C and 90°C," Scientific Basis for Nuclear Waste Management IX, M. J. Apted and R. E. Westerman, eds. Materials Research Soc., Pittsburgh, PA, 112:485-494 (1987).

7. R. J. Lemire, An Assessment of the Thermodynamic Behavior of Neptunium in Water and Model Groundwater from 25°C to 150°C, Atomic Energy of Canada Limited, Whiteshell Nucl. Res. Estbl. AECL-7817 (1984).

8. D. Rai and J. L. Ryan "Crystallinity and Solubility of PU(IV) Oxide and Hydrous Oxide in Aged Aqueous Suspensions, "Radiochem. Acta, 30:213~-216 (1982).

9. I. Puigdomenech and J. Bruno, Modelling Uranium Solubilities in Aqueous Solutions: Validation of Thermodynamic Data Base for the EQ3/6 Geochemical Codes, SKB technical report 88-21 (1988).

10. R. J. Lemire, Effects of High Ionic Strength Groundwaters on Calculated Equilibrium Concentrations in the Uranium-Water System, Atomic Energy of Canada Limited, Whiteshell Nucl. Res. Estbi. AECL-9549 (1988).

11. Code of Federal Regulations, "Disposal of High-Level Radioactive Wastes in Geological Repositories - Licensing Procedures, Title 10, Ch. 1, Pt. 60, Sec. 60.113 (1983).

# LAWRENCE LIVERMORE NATIONAL LABORATORY

LLYMP9101029
January 22, 1991

WBS 1.2.2.3.1.1
QA

SEPDB Administrator
Sandia National Laboratory
Organization 6310
P.O. Box 5800
Albuquerque NM 87185

Subject: Submission of Data to the SEPDB

Attached are a Technical Data Information Form (TDIF) and associated data for inclusion in the SEPDB. These data are taken from two reports:

1) C.N. Wilson, "Results from Cycles 1 and 2 of NNWSI Series 2 Dissolution Tests." HEDLTME85-22, May 1987.

2) C.N. Wilson, "Results from the NNWSI Series 3 Spent Fuel Dissolution Tests," PNL-7170, June 1990.

The pertinent solubility data taken after "steady-state" was reached are given in Table 1. In cases where several values from different samples with different geometries and different bumup histories were shown, the most conservative upper value is indicated. Since we don't know the cause of the scatter, it is prudent to assume the worst case, pending a better understanding of the spread in the steady-state solubilities. Where filtered and unfiltered values were available, the filtered dam were used because solubility is the information desired.

Table 2 indicates the specific source for each data value.

For slow flow of water over the spent fuel, the solubility can be used to determine the mass of each radionuclide dissolved as a function of time. Given solubilities, C, a flow rate of water contacting the spent fuel, $\Phi$, and a time, t, over which dissolution occurs, the total amount of any nuclide, i, dissolved and transported, $M_i$, is given by

$$M_i = Ci\,\Phi\,t$$

Please contact Mike Revelli of my staff at FTS 532-1982 for further information.

L. J. Jardine
LLNL Technical Project Officer
for the Yucca Mountain Project

LJJ/JB.jw

Attachments

c: C. Newbury, YMPO

Table 1. Solubility Data, Ci

| Species | Upper Limit Steady-State Concentration (µg/ml) | | |
|---|---|---|---|
| | 25°C | | 85°C |
| U | $\leq 5$ | $\leq$ | 0.5 |
| $^{239+240}Pu$ | $\leq 5 \times 10^{-3}$ | $\leq$ | $6 \times 10^{-5}$ |
| $^{241}Am$ | $\leq 3 \times 10^{-4}$ | $\leq$ | $1.5 \times 10^{-7}$ |
| $^{244}CM$ | $\leq 1.2 \times 10^{-4}$ | $\leq$ | $2.4 \times 10^{-9}$ |
| $^{237}Np$ | $\leq 4 \times 10^{-4}$ | $\leq$ | $1.4 \times 10^{-3}$ |

Only data for the solubility limited species are listed in the above table.

Table 2. Solubility Data Sources

| Species | References | |
|---|---|---|
| | 25°C | 85°C |
| U | Ref. 1, Fig. 5 | Ref. 2, Fig. 3.1 |
| $^{239+240}Pu$ | Ref. 1, Fig. 6 | Ref. 2, Fig. 3.12 |
| $^{241}AM$ | Ref. 1, Fig. 7 | Ref. 2, Fig. 3.15 |
| $^{244}CM$ | Ref. 1, Fig. 8 | Ref. 2, Fig. 3.18 |
| $^{237}Np$ | Ref. 2, Fig. 3.20 | Ref. 2, Fig. 3.20 |

Conversion factors from pCi to µg taken from Ref. 2, Table A.l.

The following describes data and an analysis procedure to obtain the release rate time response for a fully wetted mass of spent fuel dissolving without solubility limitations in water. The description is from an LLNL report UCRL-ID-107289 published in December, 1991.

Waste package analysts and designers have to understand the long term dissolution of waste form in groundwater to safely dispose of high level nuclear waste in an underground repository. The dissolution and transport processes in groundwater flow are generally considered to be the main route by which radionuclides could be released to the biosphere from a geological repository.

Many researchers have investigated the dissolution of $UO_2$, spent fuel and uraninite (a naturally occurring $UO_2$ mineral) in aqueous solutions, under either reducing or oxidizing conditions, and as a function of various other environmental variables. Experimental data on the dissolution rates of $UO_2$, spent fuel and uraninite have been reviewed by Arnell and Langmuir,[1] Parks and Pohl,[2] Bruno et al,[3] and most recently by Grambow.[4]

Important variables considered in the many investigations were pH, temperature, oxygen fugacity, carbonate/bicarbonate concentrations and other reacting media. The dissolution data are very scattered, and vary as much as six orders of magnitudes.[4] The dependence of the dissolution rates of $UO_2$, spent fuel and uraninite on these variables is not clear because of uncertainties regarding redox chemistry of uranium in solutions and in solid phases, secondary-phase formation, and surface area measurement. In addition, the previous studies were conducted under experimental conditions which were either inadequately controlled or which simulated complex repositorial conditions. The results of such studies are difficult to interpret. Several of these researchers have developed equations to correlate dissolution rates as a function of relevant variables.[5-8] However, none of the rate laws is universal, and inconsistencies or incompatibilities among the proposed laws are common.

Data indicate that $UO_2$ is easily oxidized to $U_4O_9$ and $U_3O_7$ in an air[9,10] and can be further oxidized to either $U_4O_8$ [9,10,11] or schoepite, $UO_3 \Diamond 2H_2O$.[12] The $UO_2$ surface oxidation may lead to higher leach rates because of possibly higher dissolution rates of $U_3O_7$, $U_4O_8$ or schoepite relative to that of $UO_2$[4] because of the increase of surface area of the fuels due to surface cracking.

## Discussion

We are estimating a source term for liberation of radionuclides from spent fuel dissolving under conditions of temperature and water composition related to those anticipated for a potential repository at Yucca Mountain. This is done in the same spirit as estimates that have been made for repositories in Germany[13] and Sweden.[14] It is implicit in the following treatment that fission products are dissolved congruently with the $UO_2$ fuel matrix, except for those volatile species that have partially vaporized and that fraction that has migrated to near-surface grain boundaries and are possibly dissolved independent of the matrix dissolution. Most fission products and higher actinides are distributed throughout the $UO_2$ matrix, however.

Recent measurements on $UO_2$[15] and spent fuel (SF)[16] under comparable conditions have provided dissolution rates for $UO_2$ between 25°C and 85°C in waters of various composition and for SF in deionized water (DIW) at 25°C. These experiments were done in contact with air. The results are shown in Figures 1 and 2. The rate of dissolution of SF in DIW at 25°C is 1.2-1.7 x $10^{-12}$ g $cm^{-2}$ $sec^{-1}$ This is similar to the rate for $UO_2$ in DIW at 25°C at -5 x $10^{-12}$ g $cm^{-2}$ $sec^{-1}$. Given the great variability in other reported values[4] this is reasonable agreement. In fact, the observed dissolution rate for SF at 25°C is about the same as that of $UO_2$ in (DIW + Ca + Si), a simulation of ground water.[14]

A model for dissolution is used in which the dissolution front propagates linearly in time, much like a recently published model for the advance of the oxidation front during oxidation Of $UO_2$ and spent fuel.[16-19] This implies that the particle geometry is retained. We can describe the change in characteristic dimension of a SF particle (a sort of "radius"), X as follows:

$$\mathbf{X(t) = X_0 - \left(\frac{Q}{\rho}\right)t,} \qquad (1)$$

where
- X(t) = the characteristic dimension as a function of time
- $X_o$ = the original dimension (half of the actual size)
- t = time
- Q = dissolution rate per unit area
- ρ = density

The time for complete dissolution of a particle of original size $X_o$ is then

$$t_\infty = \frac{X_o r}{Q} \qquad (2)$$

This dissolution time is proportional to size, of course, and for an ensemble of particles of different sizes, $t_\infty$ for the ensemble is that for the largest particle.

Some data are available on the size distribution of spent fuel fragments. These data are given for two different fuels but the distributions are quite similar. The aggregate of these two sets of data can be adequately described by the simplified distribution shown in Table I.

Table I

| Approximate Size (cm) ($2X_o$) | Weight (Volume Fraction |
|---|---|
| 0.15 | .02 |
| 0.25 | .14 |
| 0.35 | .29 |
| 0.50 | .38 |
| 0.70 | .17 |

Using the relationship of equation (1), we can calculate the time to dissolve a given weight (volume) fraction of an amount of SF as a function of time. For generality, we treat time as the dimensionless quantity $t/t_\infty$ with $t_\infty$ defined above. This is shown in Figure 3 for the size distribution given in Table I*, and also for a single size with $X_o$ = 0.35 cm. Here $V_o$ and V(t) are the original volume of a particle and its volume at arbitrary time, respectively. The volume is proportional to the characteristic dimension

$$V_o = kX_o^3 \text{ and } V(t) = kX^3(t)$$

where k is a constant depending on shape. Since geometry is retained, as noted above,

---

*Each size was calculated separately and the time responses were added together.

$$\frac{V(t)}{Vo} = \left(\frac{X(t)}{Xo}\right)^3 = 1 - 3\left(\frac{Q}{X_o\rho}\right)t + 3\left(\frac{Q}{X_o\rho}\right)^2 t^2 - \left(\frac{Q}{X_o\rho}\right)^3 t^3, \qquad (3)$$

$$\frac{d\left(\frac{V(t)}{V_o}\right)}{dt}$$

and the dissolution rate is -

Initially, i.e., $t \rightarrow 0$

$$\text{Rate } (t=0) = 3\left(\frac{Q}{X_o\rho}\right)$$

and the extrapolated time for total dissolution is

$$t_\infty^* = \frac{X_o\rho}{3Q}$$

In Figure 4 we show that the rate of dissolution relative to the initial rate varies with time for both the system with $X_o$ = 0.35 cm and for the distribution of Table I.

The measured dissolution rate for $UO_2$[15] and spent fuel[16] allow us to calculate actual times for dissolution. As is evident from Figure 3, the overall dissolution rate is greatest at early time and approaches zero as $t_\infty$ is approached; therefore, as a conservative approximation, we have also calculated the total dissolution time extrapolated from the initial rate, $t_\infty^*$. These times calculated for the size distribution in Table I are given in Table II. The actual dissolution rates are derived from the bottom curve in Figure 1. We chose this curve as most representative of the expected ground water. The rate equation used is

$$Q(t)(gcm^{-2}\,sec^{-1} = 6.43x10^{-9} ex - \left(\frac{4740}{RT(K)}\right) \text{ (R is in cal/mole K)} \qquad (5)$$

Table II

| Temperature (°C) $t_\infty^*$ | Dissolution Time (years) $t_\infty$ |
|---|---|
| $258.0 \times 10^3$ | $5.5 \times 10^4$ |
| $852.2 \times 10^3$ | $1.5 \times 10^4$ |

## Conclusions

These times are calculated for the case of bare fuel immersed in unlimited quantities of flowing water at flow rates sufficient to prevent any species from forming a saturated solution. Nonetheless, this estimate provides a "core" value on which to apply "credits" corresponding to features of realistic repository performance such as frequency of cladding and container failure, actual amounts of ground water and various transport rates, etc. Of course, this "core" estimate is based on only one particular dissolution rate, as is discussed above. Future measurements of dissolution rate may change this value considerably. The estimates presented here ignore the possibility that grain boundary dissolution behaves differently than bulk SF dissolution.

Dissolution tests are now under way that are designed to define the mechanism of the dissolution process Of $UO_2$ and SF in terms of oxidizing potential, temperature, pH and other water composition variables generally appropriate to a potential repository at Yucca Mountain. When these tests are completed, considerably more realistic estimates will be possible. These tests will also clarify the contribution of radionuclides from grain boundaries to the total dissolution rate.[16]

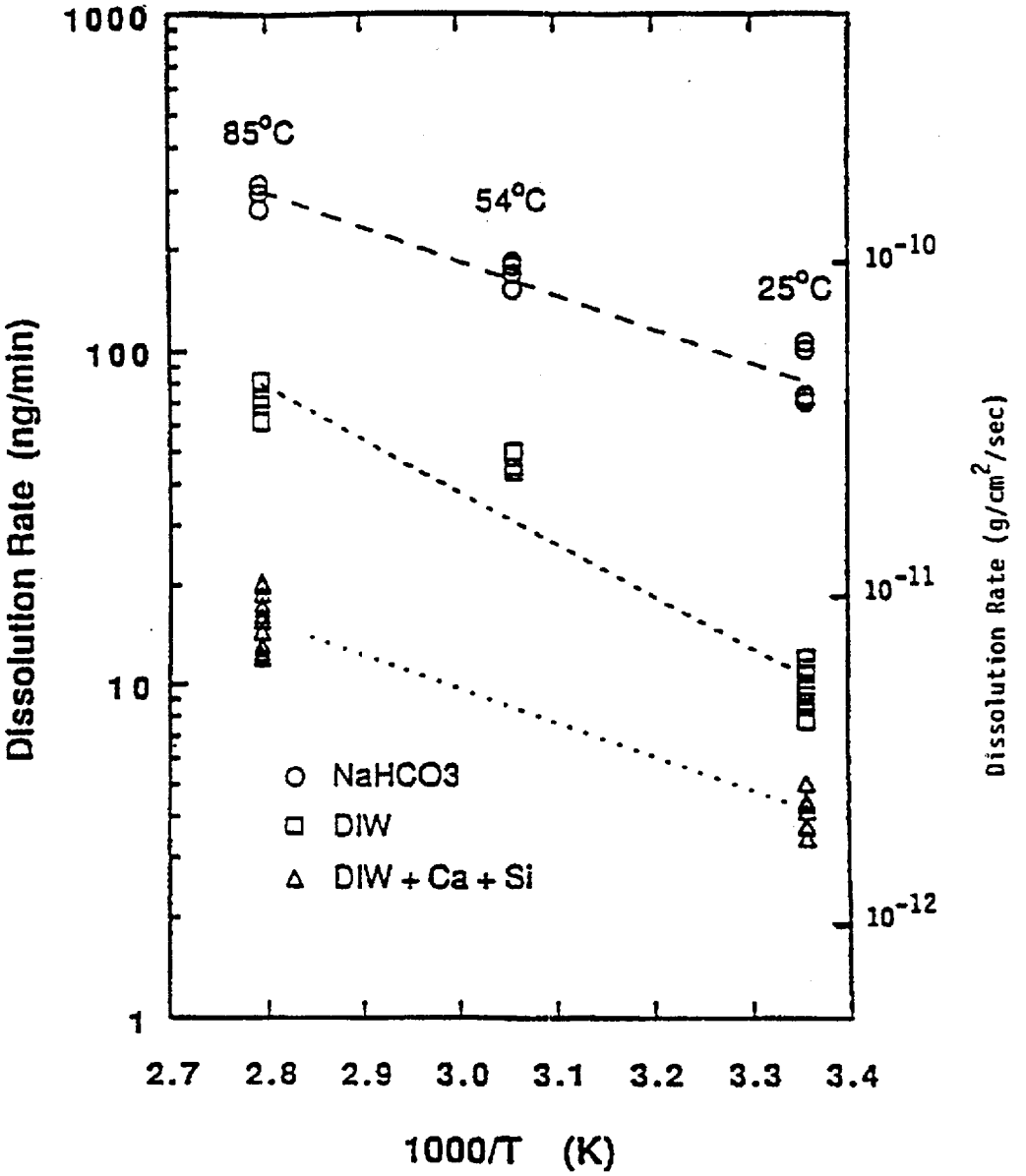


Figure 1. Arrhenius plots of the dissolution rate of $UO_2$ in waters of various composition.

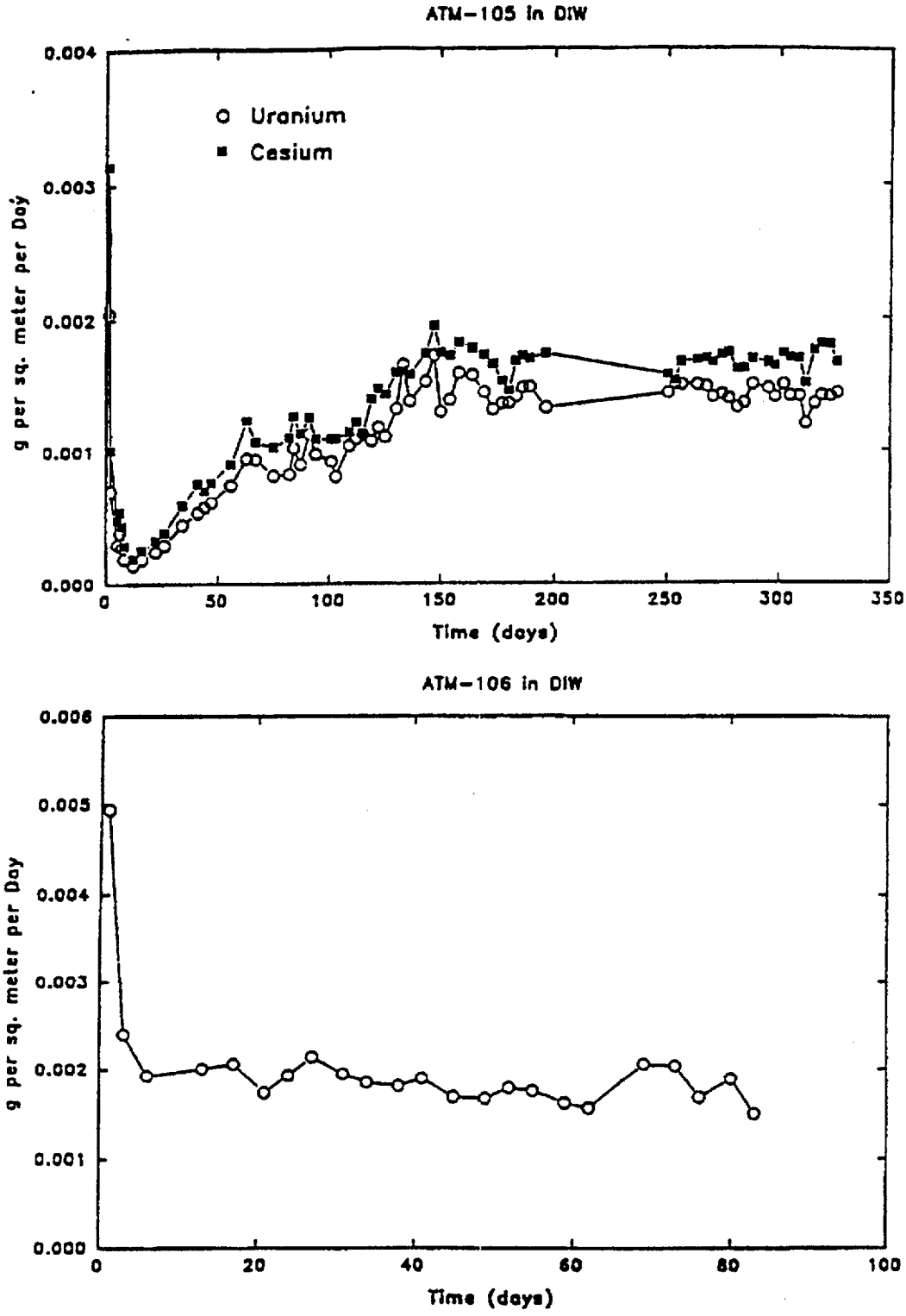


Figure 2. The approach to steady-state of the dissolution rate of two spent fuel samples.' Experiments were done at 25°C using deionized water (DIW).

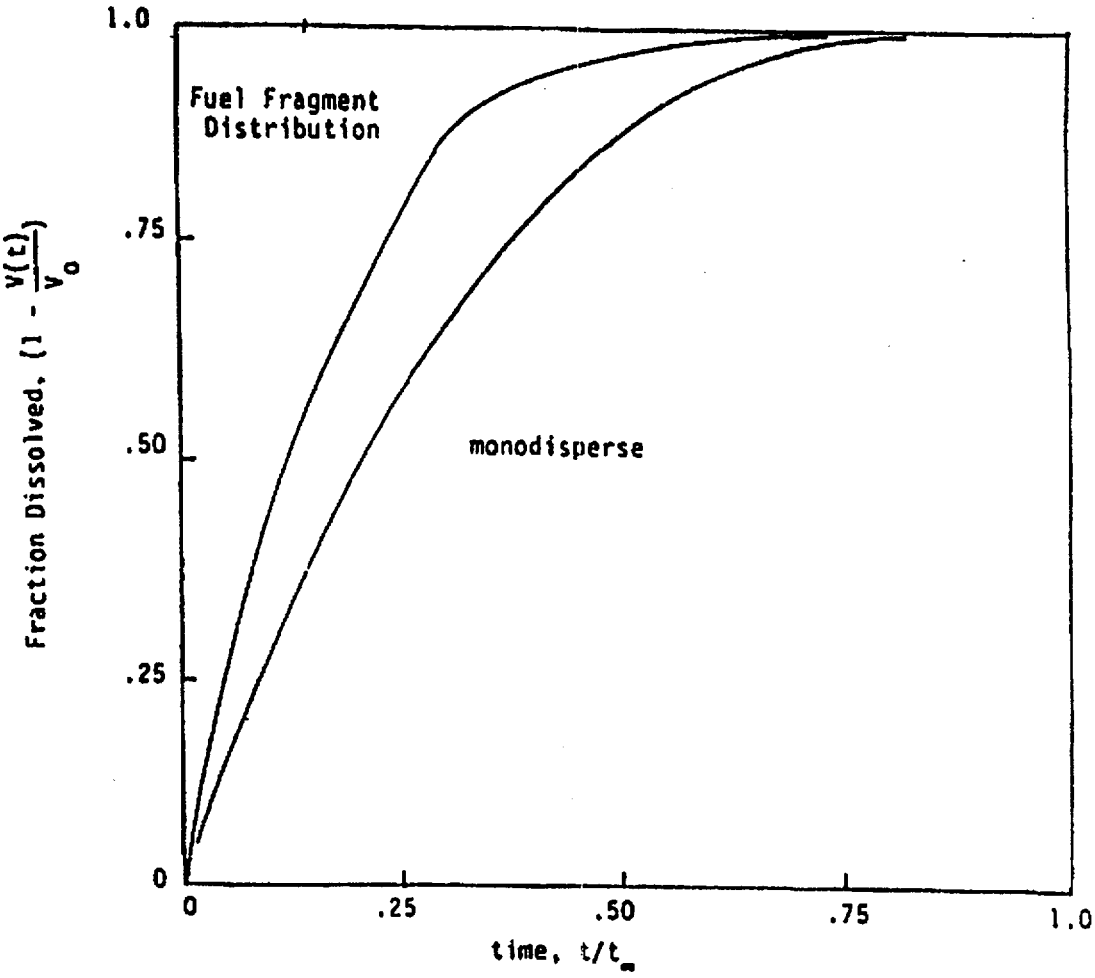


Figure 3. Calculation of the fractional dissolution in terms of dimensionless time, according to equation (3). Monodisperse refers to a single particle size.

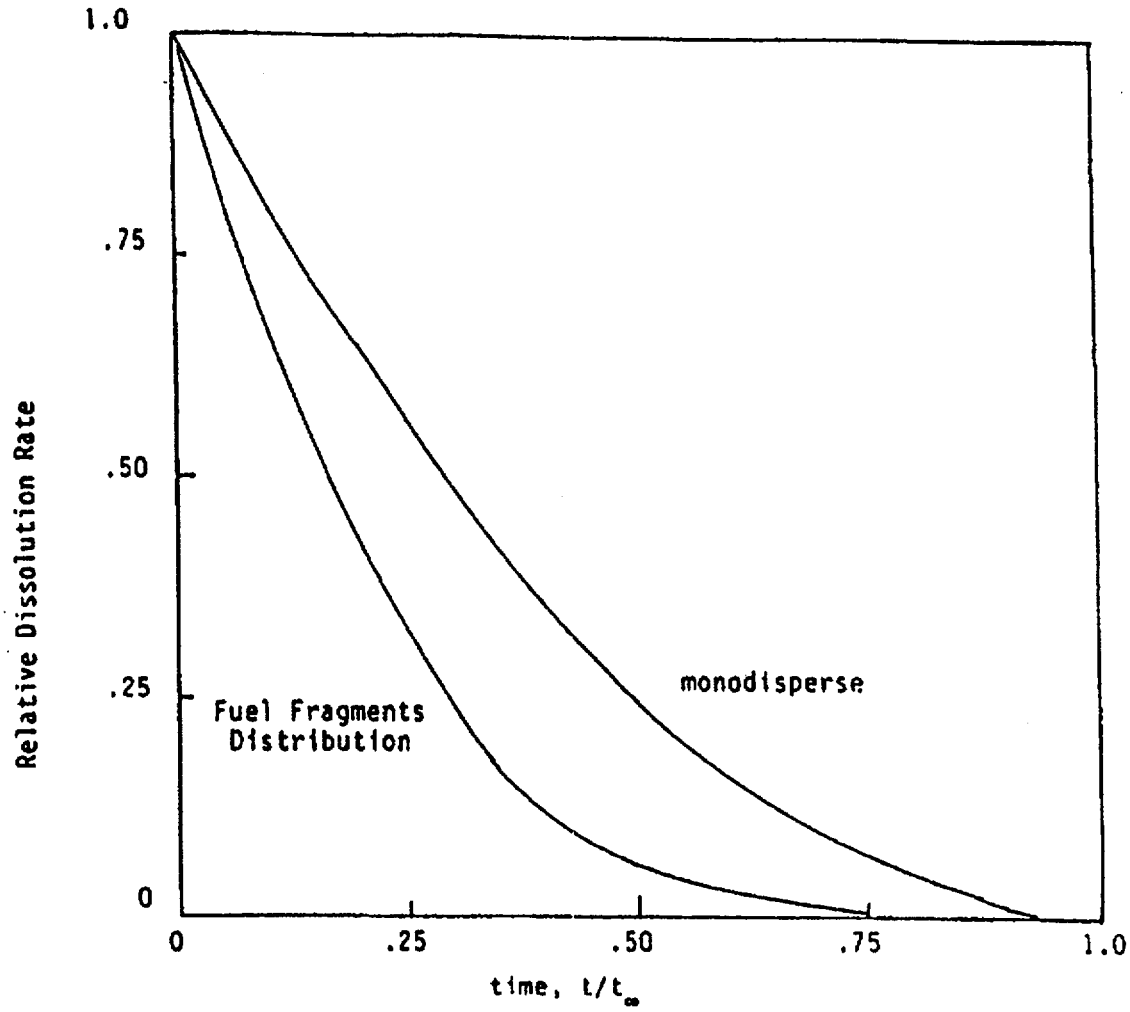


Figure 4. Evolution of the normalized dissolution rate with time as the particle size decreases, according to equation (3).

References


1. Amell, A. R., and Langmuir, D., "Factors Influencing the Solution Rate of Uranium Dioxide Under Conditions Applicable to in-Situ Leaching", Bureau of Mines Open File Report 84-79, U.S. Department of the Interior - Bureau of Mines, (1978). (Readily Available)

2. Parks, G. A., and Pohl, D. C., "Hydrothermal Solubility of Uraninite", Geochiin. Cosmochim. Acta 52 863 (1988). NNA.910821.0003

3. Bruno, J., Casas, I., and Puigdomenech, I., "The Kinetics of Dissolution of $UO_2$(s) Under Reducing Conditions", Radiochimica Acta 44/45, 11 (1988). NNA.910821.0004

4. Grambow, B., "Spent Fuel Dissolution and Oxidation. An Evaluation of Literature Data", SKB Technical Report 89-13 (1989). NNA.891013.0094

5. Grandstaff, D. E., "A Kinetic Study of the Dissolution of Uraninite", Econ. Geo. 71 1493, (1976). NNA.911025.0061

6. Schortmann, W. E. and De Sesa, M. A., "Kinetics of the Dissolution of Uranium Dioxide in Carbonate-Bicarbonate Solutions", Proc. 2nd International United Nations Conference Peaceful Uses of Atomic Energy, United Nations, Geneva, 3, 333 (1958). NNA.910821.0005

7. Pearson, R. L, and Wadsworth, M. E., "A Kinetic Study of the Dissolution of $UO_2$ in Carbonate Solution", Trans. Metal Sor. AIME 212, 294 (1958). NNA.910821.0006

8. Habashi, F., and Thurston, G. A., "Kinetics and Mechanisms of the Dissolution of Uranium Dioxide", Energ. Nucl. 14. 238 (1967). NNA.910821.0007

9. Aronson, S., "Oxidation and Corrosion of Uranium Dioxide in Uranium Dioxide: Properties and Nuclear Applications", J. Belle, ed., United States Atomic Energy Commission, 377 (1961). NNA.9110234.0060

10. Einziger, R. E., "Test Plan for Long-Term, Low-Temperature Oxidation of BWR Spent Fuel", PNL-6427, Pacific Northwest Laboratory, (1988). NNA.890224.0045

11. Aronson, S., Oxidation of $UO_2$ in Water Containing Oxygen", Bettis Tech. Rev., Westinghouse Atomic Powu Div., Report WAPD-BT-10, 93 (1958). NNA.91IM5.0062

12. Wadsten, T., "The Oxidation of Polycrystalline Uranium Dioxide in Air at Room Temperature", T. Nucl. Mat. 64, 315 (1977). (Readily Available)

13. Wvertz, R. and Ellinger, M., "Source Term for the Activity Release from a Repository for Spent LWR Fuel', Mat. Res. Soc. Symp. Proc 50, 393 (1985). (Readily Available).

14. Gray, W. and Wilson, C., "Effects of Water Composition and Temperature on the Dissolution Rate of $UO_2$' presented at 1990 Spent Fuel Workshop, Gull Harbor, Manitoba, Canada (1990). NNA.910821.0008

15. Gray, W., and Strachan, D., "Spent Fuel Grain Boundary Inventory and Testing the Congruency of $UO_2$ Matrix Dissolution of Spent Fuel", presented at the 1990 Spent Fuel Workshop, Gull Harbor, Manitoba, Canada (1990). NNA.910821.0009

16. Stout, R. B, Shaw, H. F. and Einziger, R. E., "Statistical Model for Grain Boundary and Grain Volume Oxidation Kinetics in $UO_2$ Spent Fuel", Lawrence Livermore National Laboratory UCRL-100859, September 1989. NNA.891031.0015

17. Stout, R. B., Kansa, E., Buchanan, H. C., Einziger, R. E. and Thomas, L. E., "Spent Fuel Waste Form Characteristics: Grain and Fragment Size Statistical Dependence for Oxidation Studies", Lawrence Livermore National Laboratory, UCRL-104932, December 1990. (Readily Available)

18. Stout, R. B. et al, "Spent Fuel Waste Form Characteristics: Grain and Fragment Size Statistical Dependence for Dissolution Response", Lawrence Livermore National Laboratory Report UCRL-104931, December 1990. (Readily Available)

19. Van Luik, A. E, et al, "Spent Nuclear Fuel as a Waste Form for Geologic Disposal: Assessment and Recommendations on Data and Modeling Needs, Pacific Northwest Laboratory Report, PNL-6329 (UC-70), September 1987. (Readily Available)